Cell Reports

Article

Insect-transmitted plant virus balances its vertical transmission through regulating Rab1-mediated receptor localization

Graphical abstract

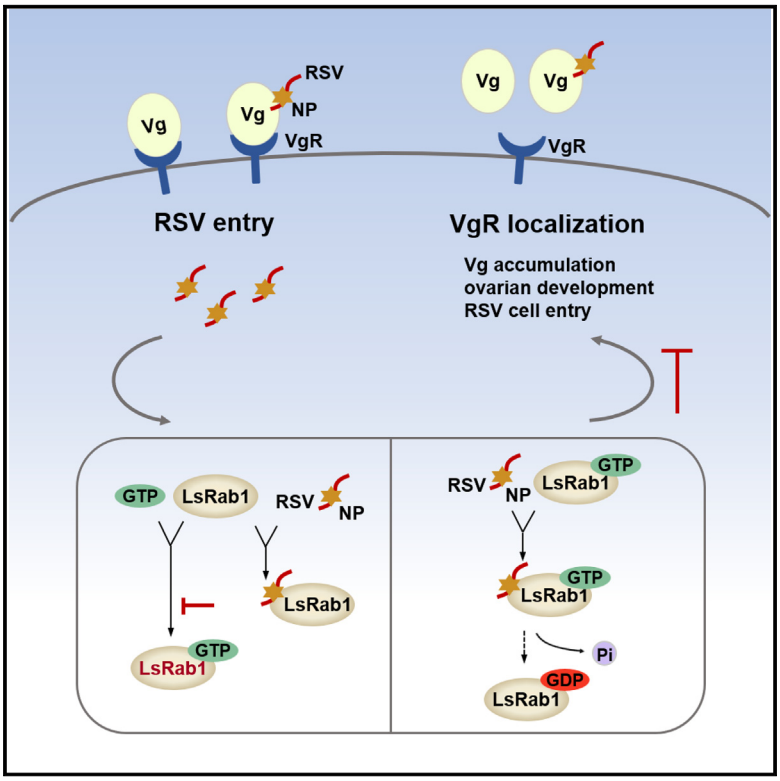

Highlights

- RSV inhibits continuous ovarian cell infection by disrupting VgR localization
- RSV NP interacts with LsRab1 in *L. striatllus* ovaries, preventing proper VgR trafficking
- NP inhibits LsRab1 function by blocking GTP binding and stimulating GTP hydrolysis

Authors

Qing Liu, Xiangyi Meng, Zhiyu Song, ..., Rongxiang Fang, Yan Huo, Lili Zhang

Correspondence

huoy@im.ac.cn (Y.H.),
zhangll@im.ac.cn (L.Z.)

In brief

Liu et al. demonstrate that after RSV enters ovarian nurse cells, its NP binds to insect Rab1, inactivating Rab1's function in VgR trafficking and limiting continuous viral infection. This RSV NP-Rab1 interaction in ovaries creates a balance that ensures both vector offspring survival and viral vertical transmission.

Liu et al., 2024, Cell Reports *43*, 114571
August 27, 2024
https://doi.org/10.1016/j.celrep.2024.114571

CellPress

Cell Reports

CellPress
OPEN ACCESS

Article

Insect-transmitted plant virus balances its vertical transmission through regulating Rab1-mediated receptor localization

Qing Liu,[1,3,5] Xiangyi Meng,[1,3,5] Zhiyu Song,[1,3] Ying Shao,[4] Yao Zhao,[1,3] Rongxiang Fang,[1,2,3] Yan Huo,[1,2,*] and Lili Zhang[1,2,6,*]

[1]State Key Laboratory of Plant Genomics, Institute of Microbiology, Chinese Academy of Sciences, Beijing 100101, China
[2]CAS Center for Excellence in Biotic Interactions, University of Chinese Academy of Sciences, Beijing 100049, China
[3]University of the Chinese Academy of Sciences, Beijing 100049, China
[4]College of Veterinary Medicine, Shanxi Agricultural University, Jinzhong, Shanxi Province 030801, China
[5]These authors contributed equally
[6]Lead contact
*Correspondence: huoy@im.ac.cn (Y.H.), zhangll@im.ac.cn (L.Z.)
https://doi.org/10.1016/j.celrep.2024.114571

SUMMARY

Rice stripe virus (RSV) establishes infection in the ovaries of its vector insect, *Laodelphax striatellus*. We demonstrate that RSV infection delays ovarian maturation by inhibiting membrane localization of the vitellogenin receptor (VgR), thereby reducing the vitellogenin (Vg) accumulation essential for egg development. We identify the host protein *L. striatellus* Rab1 protein (LsRab1), which directly interacts with RSV nucleocapsid protein (NP) within nurse cells. LsRab1 is required for VgR surface localization and ovarian Vg accumulation. RSV inhibits LsRab1 function through two mechanisms: NP binding LsRab1 prevents GTP binding, and NP binding LsRab1-GTP complexes stimulates GTP hydrolysis, forming an inactive LsRab1 form. Through this dual inhibition, RSV infection prevents LsRab1 from facilitating VgR trafficking to the cell membrane, leading to inefficient Vg uptake. The Vg-VgR pathway is present in most oviparous animals, and the mechanisms detailed here provide insights into the vertical transmission of other insect-transmitted viruses of medical and agricultural importance.

INTRODUCTION

Most plant viruses are transmitted by insect vectors, while some of these viruses can be transmitted vertically from parents to offspring, resulting in naturally infected insects.[1–4] This mechanism increases the infection rate in insect populations and helps the viruses survive harsh winter conditions.[5–9] Rice stripe virus (RSV) is the causative agent of rice stripe disease and is completely dependent on insect vectors for transmission between crops, with the small brown planthopper (SBPH, *Laodelphax striatellus*) being the primary vector.[10] Previous studies have revealed the persistent-propagative transmission manner of RSV by *L. striatellus*. When RSV-free *L. striatellus* feeds on RSV-infected rice plants, the virus enters the insect guts and initiates its entry from the midgut epithelium.[11,12] The virus then replicates and spreads throughout the midgut and other gut tissues. The viruses then overcome the gut barrier and enter the hemolymph, where RSV can invade various tissues.[13] Among these, RSV invades the salivary glands and spreads horizontally to healthy plants during insect feeding[14–16] and invades female ovaries to spread vertically to offspring.[17,18]

RSV is a type member of the genus *Tenuivirus*, belonging to the family Phenuiviridae in the order Bunyavirales.[19] The RSV genome consists of four single-stranded RNA segments, encoding seven proteins: RNA-dependent RNA polymerase (RdRp), P2 protein, glycoprotein Pc2, viral gene-silencing suppressor P3, nucleocapsid protein NP (Pc3), nonstructural disease-specific protein P4, and movement protein Pc4. The RSV ribonucleoproteins (RNPs) are the minimal infectious units and consist of NP and a small number of RdRp proteins.[20,21] NP is the sole structural protein of RSV virions and has been revealed to play a crucial role in mediating viral cell entry.[17,18,22]

In our previous studies, we have addressed the vertical transmission mechanism of RSV by *L. striatellus*. RSV NP binds to *L. striatellus* vitellogenin (Vg) in the hemolymph, hitchhiking the Vg transport pathway to invade the developing ovaries. Vg is an indispensable protein for the embryonic development of almost all oviparous animals, and its transport pathway remains relatively conserved across various animals.[23,24] Vg is synthesized extra-ovarially and taken up by ovarian cells through Vg receptor (VgR)-mediated endocytosis.[17,18,22] The conservation of the Vg transport from hemolymph to ovary suggests that this ligand-receptor interaction-mediated virus transmission pathway may be utilized by various arthropod-transmitted plant and animal viruses. For instance, the coat protein of tomato yellow leaf curl virus binds to whitefly Vg, enabling viral transovarial

transmission.[25] In *Drosophila melanogaster*, VgR facilitates the ovarian entry of the endogenous retrovirus ZAM.[26] Although the role of the Vg-VgR pathway in mediating virus vertical transmission has been studied in several insect-virus interaction systems, the intracellular molecular events after the virus infecting the ovary remain largely unexplored.

Rab proteins belong to the Ras-like small GTPase superfamily and act as molecular switches that regulate intracellular substance trafficking in all eukaryotic cells by alternating between the GTP and GDP binding states.[27–29] Rab1 is a specific member of the Rab protein family that plays a crucial role in regulating vesicular transport between the endoplasmic reticulum (ER) and the Golgi apparatus.[30–36] When Rab1 is in its GTP-bound form, it interacts with a variety of effector proteins that are involved in vesicle tethering, docking, and fusion. This allows for the efficient transport of cargo proteins and lipids from the ER to the Golgi apparatus. Studies have shown that Rabs play a crucial role in regulating the transport of cellular receptors.[37–43] For instance, in neonatal rat ventricular myocytes, Rab1 has been found to facilitate the ER-to-Golgi trafficking of a1-adrenergic receptors, thereby regulating their cell-surface targeting.[39] Similarly, in murine bone marrow-derived macrophages, Rab1 has been shown to modulate TLR4 traffic from the ER to the Golgi apparatus, promoting its cell-surface expression.[41] Additionally, Rab1 is directly or indirectly involved in virus infection or replication.[34,44–46] For example, in hepatocytes, Rab1b regulates the ER-to-Golgi transport of the very-low-density lipoprotein components ApoE and ApoB100, thus affecting the secretion of hepatitis C virus.[47]

In this work, we uncovered a direct interaction between *L. striatellus* Rab1 (LsRab1) and RSV NP in ovaries. RSV binding retains LsRab1 in an inactive molecular form, inhibiting its intracellular trafficking function. As a result, membrane localization of VgR, which mediates RSV ovarian entry via Vg, is reduced. This decreases Vg uptake and delays ovarian development. Aligned with the decreased Vg cell entry, RSV ovarian infection was also decreased. Through this self-limiting mechanism, RSV can infect *L. striatellus* ovaries to reach vertical transmission without impairing the ovaries due to a heavy viral load. Our findings provide detailed molecular insight into the processes occurring in insect ovarian cells following viral infection.

RESULTS

RSV NP binds and colocalizes with the host factor LsRab1 in ovarian nurse cells

Our previous study revealed that RSV NP binds to Vg in *L. striatellus* hemolymph, and the virus subsequently invades ovarian nurse cells via VgR-mediated endocytosis.[17,18,22] To investigate intracellular events following RSV entry into ovarian cells, we performed co-immunoprecipitation (coIP) to identify host proteins interacting with RSV NP. This revealed a potential association with the Ras-related GTPase Rab-1A (Tables S1 and S2; Figure S1A), known to function in receptor trafficking. Further genomic[48] and phylogenetic analyses uncovered that the *L. striatellus* genome encodes 27 potential Rab proteins (Table S3). *Rab-1A* exists as a single-copy ortholog in *L. striatellus*, designated *LsRab1* (GenBank: RZF47397.1) (Figures S1A and S1B; Table S3). Bioinformatic predictions support LsRab1 being a cytoplasmic protein. RT-qPCR analysis in different SBPH developmental stages and different tissues indicated that the *LsRab1* gene is predominantly expressed in ovaries and midguts with adults showing higher expression levels compared to larvae (Figures S1C–S1E).

We performed coIP to verify the interaction between RSV and LsRab1 (Figure 1A). We then conducted GST pull-down and microscale thermophoresis (MST) assays to validate the LsRab1-RSV NP interaction. Recombinantly expressed, His-tagged LsRab1 specifically bound GST-fused NP but not GST alone (Figure 1B). MST analysis determined their binding affinity to be 7.59 ± 1.22 μM, while LsRab1 does not interact with the control protein thioredoxin A (TrxA, Figure 1C). For localization within infected ovaries, immunofluorescence assay (IFA) revealed LsRab1 and RSV colocalizing in germarium nurse cells—the initial site of ovarian invasion (Figure 1D).

To confirm the detailed direct interaction between RSV NP and LsRab1, we constructed LsRab1 truncations. AlphaFold2 was used to predict the interaction region among RSV NP and LsRab1, revealing that RSV NP mainly binds to the N-terminal domain of LsRab1 (Figure S2). Consequently, we constructed two truncated LsRab1 proteins: the N-terminal protein, NLsRab1, containing amino acids 1–101, and the C-terminal protein, CLsRab1, containing amino acids 102–204. Pull-down experiments were performed to detect the interaction between recombinantly expressed RSV NP and NLsRab1/CLsRab1, indicating that RSV NP can specifically bind to the NLsRab1 but not CLsRab1 (Figure 1E), supporting the specific interaction between RSV NP and the LsRab1 N-terminal region.

Collectively, these data confirm that LsRab1 directly interacts with RSV NP *in vitro* and colocalizes *in vivo* within nurse cells during early viral infection.

LsRab1 is necessary for RSV to infect *L. striatellus* ovaries

To determine the effect of LsRab1 on RSV ovarian infection, we performed LsRab1 knockdown mediated by RNA interference (RNAi). *LsRab1*-specific dsRNA (dsLsRab1) or control dsgfp was delivered into the hemolymph of RSV-infected 5th-instar nymphs. At 48 h post eclosion (hpe), we quantified viral loads in the ovaries by RT-qPCR and IFA. RT-qPCR analysis confirmed efficient mRNA knockdown by dsLsRab1, with near complete loss of LsRab1 protein by western blotting (Figures 2A and 2B). Aligned with this, dsLsRab1 treatment significantly decreased ovarian RSV titers compared to control insects (Figures 2C and 2D).

Further examination by confocal microscopy revealed distinct infection patterns following LsRab1 knockdown. In control dsgfp insects, RSV extensively invaded most germarium nurse cells. However, dsLsRab1 treatment strongly inhibited nurse cell infection. We designated ovaries with germarium infection as type I and those without germarium infection as type II (Figure 2E). In both dsLsRab1 and control groups, abundant RSV was localized to the pedicel region, which is not an ovarian entry site. As the pedicel-localized viruses also contribute to the total viral titers quantified by RT-qPCR/western blots, the inhibition of nurse cell infection caused by LsRab1 knockdown is likely more severe

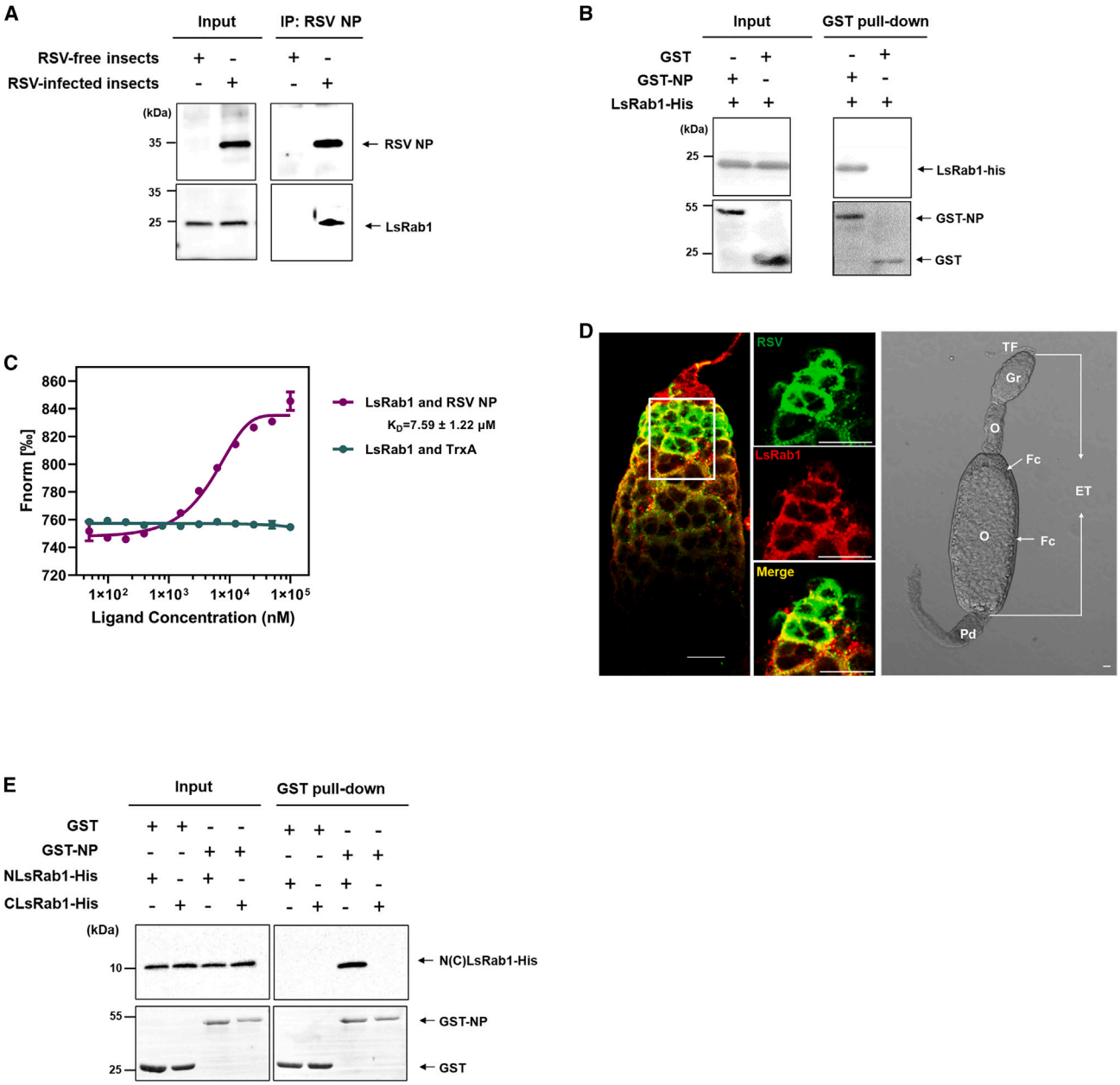

Figure 1. Interaction between LsRab1 and RSV NP

(A) Co-immunoprecipitation (coIP) assay identifying LsRab1 interacting with the RSV NP. RSV NP antibodies were the baits for capturing native interaction proteins with RSV in RSV-infected insects. RSV-free insects were used as the control.

(B) GST pull-down assays showing the interaction between RSV NP (GST-NP) and LsRab1 (LsRab1-His). GST was used as a negative control.

(C) MST assays showing the interaction between LsRab1 and RSV NP. TrxA was used as a negative control to interact with LsRab1. Bars represent standard deviation (SD).

(D) Immunofluorescence assay showing the co-localization of RSV and LsRab1 in the *L. striatellus* germarium nurse cells. RSV was probed with rabbit anti-RSV antibody and stained with Alexa Fluor 488 (shown in green). LsRab1 was probed with mouse anti-LsRab1 antibody and stained with Alexa Fluor 568 (shown in red). Images were examined using a Leica TCS SP8 confocal microscope. Images are representative of three independent experiments with a total of 12 SBPHs analyzed. The scale bar represents 20 μm. Schematic diagrams of the *L. striatellus* ovary structure are shown on the right, with nurse cells located in the germarium region. The scale bar represents 100 μm. TF, terminal filament; ET, egg tube; Gr, germarium; O, oocyte; Pd, pedicel; Fc, follicular cell.

(E) GST pull-down assays showing the interaction between RSV NP and the truncated LsRab1 proteins NLsRab1 and CLsRab1. NLsRab1, the N-terminal protein, contains LsRab1 amino acids 1–101, and CLsRab1, the C-terminal protein, contains amino acids 102–204. GST was used as a negative control.

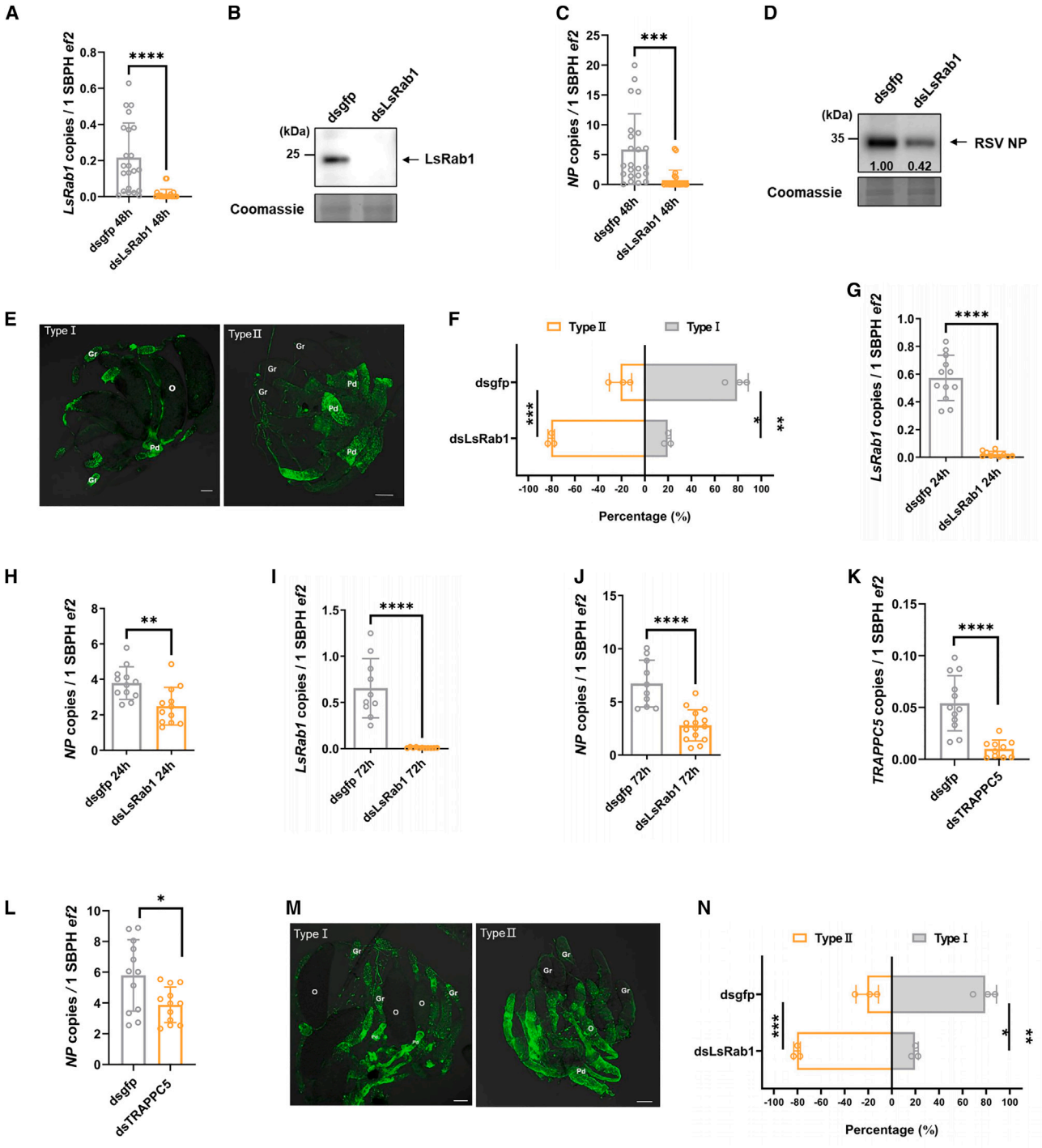

Figure 2. LsRab1 deficiency reduces RSV infection of the ovary

(A–D) *LsRab1*-specific dsRNA (dsLsRab1) or *gfp*-specific dsRNA (dsgfp) was microinjected into the hemolymph of RSV-infected 5th instar nymphs. At 48 h post eclosion (hpe), mRNA and protein levels were measured by RT-qPCR (A and C) and western blotting (B and D), respectively.

(E) Immunofluorescence assay depicting different RSV infection levels in *L. striatellus* ovarioles. Type I: abundant RSV (green) distributed in the germarium; type II: RSV primarily localized in the pedicel.

(F) Classification summary of *L. striatellus* ovaries with different RSV infection levels in dsgfp- or dsLsRab1-treated insects.

(G–J) RT-qPCR showing the influence of dsLsRab1 or dsgfp treatment on gene expression and ovarian RSV infection at different time points, including 24 and 72 hpe.

(legend continued on next page)

than these titers indicate (Figures 2C–2E). Indeed, quantitative analysis confirmed a reduction from 79% type I ovaries in control insects down to 20% after dsLsRab1 knockdown (Figure 2F), indicating strong viral inhibition by dsLsRab1 deficiency.

We also measured the influence of LsRab1 deficiency on RSV infection at 24 and 72 hpe. RT-qPCR analysis revealed that dsLsRab1 treatment significantly decreased ovarian RSV titers at these different time points (Figures 2G–2J).

The activity of Rab proteins requires guanine nucleotide exchange factors (GEFs). To further confirm the function of LsRab1 in influencing RSV ovarian infection, we investigated its GEF function. Previous studies have shown that the transport protein particle (TRAPP) complex serves as a GEF for Rab1.[49] By searching the *L. striatellus* genome, we identified orthologs of all six *Drosophila melanogaster* TRAPP core subunits, with their sequence identities detailed in Table S4. Four of these subunits (TRAPPC1, TRAPPC3, TRAPPC4, and TRAPPC5) are minimally required to activate Rab GTPase activity. TRAPPC5 plays a crucial role in allosterically regulating the TRAPP interaction interface with Rab proteins. A TRAPP subcomplex lacking the TRAPPC5 subunit has impaired GEF activity.[50] Therefore, we focused on TRAPPC5 to further confirm LsRab1's function in facilitating RSV ovarian infection. We knocked down the expression of *TRAPPC5* in 5th-instar RSV-infected nymphs. RT-qPCR was performed at 48 hpe to confirm the knockdown efficiency (Figure 2K). We found that following the deficiency of *TRAPPC5*, RSV infection levels in the ovaries were significantly reduced (Figures 2L and 3H). Confocal microscopy further confirmed that dsTRAPPC5 treatment strongly inhibited nurse cell infection, and most viruses were located in the pedicel (Figures 2M and 2N). These results are consistent with those of *LsRab1* deficiency, further indicating the function of LsRab1 in facilitating RSV ovarian infection.

Taken together, these results demonstrate that *LsRab1* deficiency impairs RSV ovarian infection, supporting an essential role for LsRab1 in initial viral infection.

LsRab1 deficiency inhibits ovarian development, Vg accumulation, and the cell-surface localization of ovarian VgR

LsRab1 deficiency also notably hindered ovarian development (Figure 3A). DsLsRab1 or dsgfp was injected into the hemolymph of RSV-infected 5th-instar nymphs. Ovarian development at 48 hpe was detected by confocal microscopy. Compared to dsgfp controls, dsLsRab1 treatment resulted in delayed ovarian development (Figure 3A). The egg tubes of the ovary were substantially smaller, and the vitellogenin deposition was negligible in oocytes. Western blotting corroborated near complete loss of ovarian Vg accumulation in ovaries upon LsRab1 deficiency (Figure 3B). To determine if impaired ovarian Vg resulted from reduced extra-ovarian synthesis, we measured Vg expression. RT-qPCR indicated comparable *Vg* mRNA levels in the fat body and hemocytes between groups (Figure S3A). Moreover, Vg abundance in hemolymph was unchanged by dsLsRab1 injection (Figure S3B). These results indicate an essential role of LsRab1 in promoting ovarian development and accumulation of extra-ovarian-derived Vg, independent of *de novo* Vg synthesis.

Vg is extra-ovarian synthesized and transported into ovaries via VgR-mediated endocytosis. Given prior associations of Rab1 with receptor trafficking,[37–39] we investigated if LsRab1 deficiency inhibits VgR transport to the cell surface. Flow cytometry staining was conducted to differentiate between VgR-positive ovarian cells (VgR^{+}) and VgR-negative cells (VgR^{-}). Thirty ovaries were dissected from the dsgfp- or dsLsRab1-treated insects and then digested into single cells using elastase and collagenase. VgR-specific antibodies were used to label the VgR proteins localized on the ovarian cell surface. Compared to controls, the dsLsRab1 treatment group had significantly fewer ovarian cells with VgR fluorescence values between 10^5–10^7 (Figures 3C and 3D). After statistics, it was found that dsLsRab1 treatment resulted in a 2.39-fold reduction in the percentage of VgR^{+} cells compared to dsgfp treatment (Figure 3E). We further confirmed decreased VgR membrane localization by cell fractionation and western blotting. The cytomembrane was separated from the cytoplasm, and western blotting was performed to detect VgR distribution. DsLsRab1 treatment resulted in less membrane-associated VgR and more cytoplasmic VgR compared to dsgfp treatment (Figures 3F and 3G), supporting that LsRab1 is necessary for VgR's intracellular transport.

To exclude the possibility that the decreased percentage of the VgR^{+} cells was caused by decreased VgR synthesis, we performed RT-qPCR and western blotting to measure VgR mRNA and protein levels. The ovaries at 48 hpe were measured. RT-qPCR indicated that *VgR* mRNA levels were not affected by LsRab1 deficiency (Figure S3C), and western blotting showed that LsRab1 deficiency did not affect VgR protein levels (Figure S3D). In addition, MST assay revealed that LsRab1 does not directly interact with the VgR cytoplasmic region (VgR-CP) (Figure S4).

To further confirm the LsRab1 function in mediating Vg uptake, VgR localization, and ovarian development, we knocked down the expression of TRAPPC5. The gene knockdown was performed on the 5th-instar RSV-infected nymphs. Western blotting was performed to measure protein localization. We found that following the deficiency of TRAPPC5, the ovarian Vg was dramatically decreased (Figure 3H), and VgR localization on the cytomembrane was also significantly decreased (Figure 3I). As a result, ovarian development was also heavily inhibited (Figure 3J). These results are consistent with those of LsRab1

(K and L) RT-qPCR showing gene-silencing efficiency of *TRAPPC5* in ovaries (K) and RSV infection level (L). *TRAPPC5*-specific dsRNA (dsTRAPPC5) or dsgfp was microinjected into the hemolymph of RSV-infected 5th instar nymphs. Measurements were taken in females at 48 hpe.

(M) Immunofluorescence assay illustrating different RSV infection levels in *L. striatellus* ovarioles. Type I: abundant RSV (green) distributed in the germarium; type II: RSV primarily localized in the pedicel.

(N) Classification summary of *L. striatellus* ovaries with different RSV infection levels in dsgfp- or dsTRAPPC5-treated insects. Each dot represents ovaries from three RSV-infected insects. Mean and SD were calculated from three independent dsRNA microinjections. RSV was immunolabeled with rabbit anti-RSV antibody and stained with Alexa Fluor 488. Gr, germarium; O, oocyte; Pd, pedicel; scale bar, 100 μm. *$p < 0.05$; **$p < 0.01$; ***$p < 0.001$; ****$p < 0.0001$.

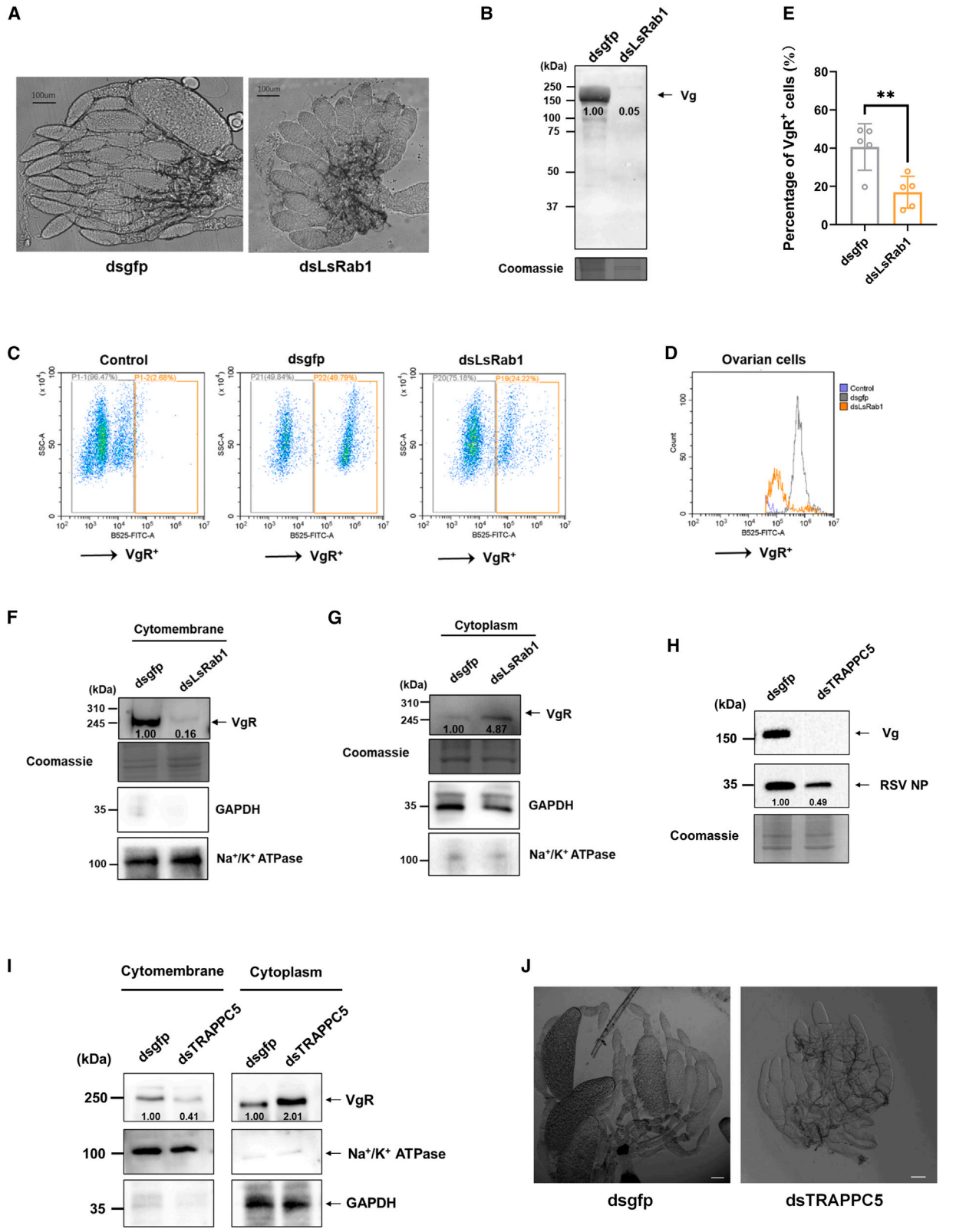

(legend on next page)

deficiency, further indicating the function of LsRab1 in ovarian development.

Together, these results support that LsRab1 is necessary for ovarian development. The reduced VgR surface localization after LsRab1 knockdown is the decisive reason for the reduced Vg accumulation in ovaries. On the other hand, these results also support that LsRab1 may facilitate RSV ovarian infection (Figure 2) by enabling VgR to localize to the cell surface.

RSV infection delays ovarian development and reproduction by reducing VgR surface localization

We have demonstrated that RSV NP proteins bind LsRab1 and that LsRab1 is necessary for VgR localization to the cell surface. This led us to hypothesize that RSV infection may also alter VgR localization in ovarian nurse cells, thereby influencing Vg uptake and ovarian development.

To investigate the influence of RSV ovarian infection on *L. striatellus* ovarian development, we compared ovarian development between RSV-free and infected females. Based on Vg accumulation inside the ovary, we classified ovaries at 48 hpe into three types (Figure 4A): type I had no obvious Vg accumulation; type II had Vg accumulation in some oocytes but no mature eggs; type III contained some mature eggs in the tubules. We found that RSV infection significantly delayed ovarian development. Among the ovaries of RSV-free insects, 41.78% ± 7.58% were type III, 35.22% ± 5.58% type II, and only 17.44% ± 8.14% type I. In comparison, 49.87% ± 13.44% of RSV-infected insects had type I ovaries, with 16.02% ± 6.60% type III and 34.10% ± 8.69% Type II (Figure 4B). This indicates RSV ovarian infection inhibits ovarian development.

In line with delayed ovarian development, we found decreased Vg accumulation specifically in RSV-infected ovaries compared to controls (Figure 4C). Moreover, *Vg* expression in fat body/hemocytes and Vg protein levels in the hemolymph were not decreased (Figures S5A and S5B), indicating the reduction in Vg ovarian accumulation was not due to decreased Vg synthesis. Instead, we hypothesized that Vg ovarian entry was impaired upon infection.

To directly test if RSV infection impacts VgR localization, we performed flow cytometry on single ovarian cells from RSV-free and infected females at 48 hpe, when the germarium nurse cells are almost fully infected. Thirty ovaries were dissected from the RSV-free or infected insects and digested into single cells. VgR-specific antibodies labeled surface VgR proteins on ovarian cells. Compared to RSV-free insects, the infected group had significantly fewer VgR^+ ovarian cells (Figures 4D and 4E). RSV infection resulted in a 1.89-fold reduction in the percentage of VgR^+ cells compared to RSV-free insects (Figure 4F). We further confirmed decreased membrane VgR by cell fractionation and western blotting, finding less membrane and more cytoplasmic VgR compared to the uninfected insects (Figure 4G), supporting that RSV infection inhibits VgR's cytomembrane localization. RT-qPCR revealed that *VgR* mRNA levels at 48 hpe were unaffected by RSV infection (Figure S5C), indicating that the decreased membrane VgR was not due to reduced VgR synthesis.

To investigate the impact of altered VgR localization on insect reproduction and nymph emergence, we conducted a comparative analysis between RSV-free and RSV-infected *L. striatellus*. Our results demonstrated that RSV infection significantly delayed both insect reproductive processes and nymph emergence. RSV-free females initiated egg production at 4 days post eclosion (dpe), with nymph emerging from these eggs starting at 10 dpe. In comparison, RSV-infected females exhibited a delayed timeline, with egg production beginning at 5 dpe and nymph emergence occurring from 12 dpe onward. Furthermore, we observed a consistent and significant difference in reproductive output between the two groups. At each time point (dpe), the RSV-free group produced substantially higher numbers of eggs and emerged nymphs compared to their RSV-infected counterparts (Figure 4H).

RSV NP inhibits LsRab1 activation by blocking GTP binding or stimulating GTP hydrolysis

Since RSV alters VgR localization and LsRab1 functions in receptor trafficking, we investigated whether RSV regulates LsRab1 activity. Rab proteins exert molecular switching functions by cycling between a GTP-bound active form and a GDP-bound inactive form.[24] We first tested the ability of recombinantly expressed LsRab1 to bind GTP and GDP *in vitro* using MST assays. The results showed that LsRab1 can directly interact with GTP and GDP with K_D values of 0.71 ± 0.43 μM and 12.35 ± 0.74 μM, respectively (Figures 5A and 5B). Previous studies have revealed that the $Rab1^{S22N}$ and $Rab1^{N121I}$ mutants

Figure 3. LsRab1 deficiency delays ovarian development by decreasing VgR surface localization

(A) Microscope showing the ovarian development status at 48 hpe in dsgfp- or dsLsRab1-treated insects. Scale bar, 100 μm.

(B) Western blotting showing Vg ovarian accumulation in dsgfp- or dsLsRab1-treated insects. Coomassie was used as a reference for sample loading.

(C) Flow cytometry staining to differentiate VgR^+ and VgR^- ovarian cells. The VgR^+ or VgR^- ovarian cells represent the ovarian cells with or without cell-surface localized VgR proteins. Ovarian cells incubated without specific primary antibodies were used as a control.

(D) The number of VgR^+ cells corresponding to different fluorescence intensities in dsLsRab1- and dsgfp-treated insects.

(E) Calculation of the percentages of the VgR^+ ovarian cells in dsLsRab1- and dsgfp-treated insects. Mean and SD were calculated from three independent biological replicates. $^{**}p < 0.01$.

(F and G) Western blotting showing VgR protein levels in cytomembrane (F) and cytoplasmic (G) protein extracts of insect ovaries. The transmembrane protein Na^+/K^+ ATPase and the cytoplasmic enzyme GAPDH are markers distinguishing the cytomembrane from the cytoplasm. Coomassie staining indicates the sample loading.

(H) Western blotting showing Vg and RSV NP ovarian accumulation in dsgfp- or dsTRAPPC5-treated insects. Coomassie was used as a reference for sample loading.

(I) Western blotting showing VgR protein levels in cytomembrane and cytoplasmic protein extracts of insect ovaries.

(J) Microscope showing the ovarian development status at 48 hpe in dsgfp- or dsTRAPPC5-treated insects. Scale bar, 100 μm. The figures shown are representative of three independent biological replicates.

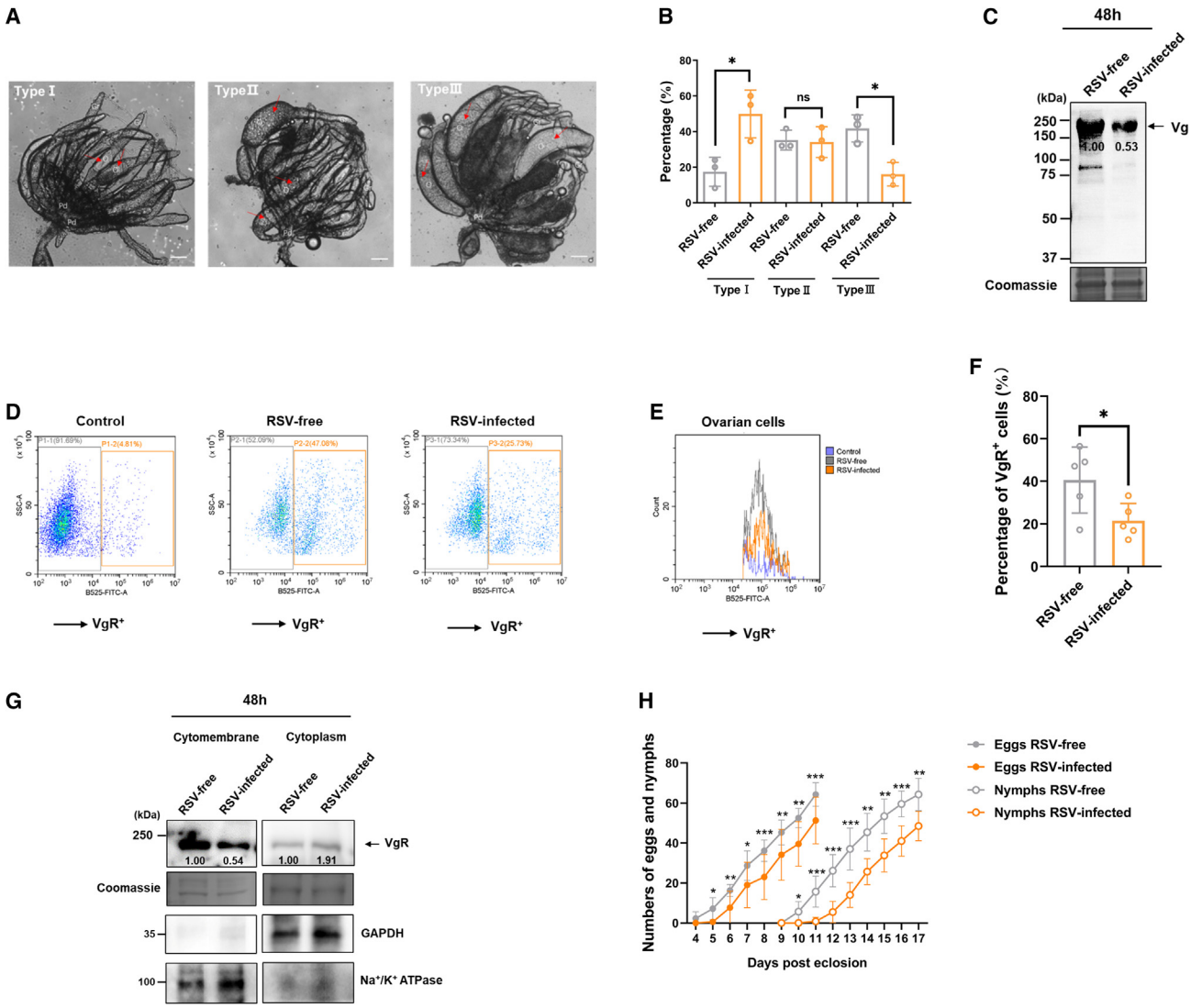

Figure 4. RSV infection delays ovarian development by reducing VgR membrane localization and Vg uptake

(A) Microscopy to define different ovarian development at 48 hpe. Type I ovaries had no obvious Vg accumulation in oocytes, type II ovaries had Vg accumulation in some oocytes but contained no mature eggs, and type III ovaries contained some mature eggs in the tubules. Red arrows indicate the developing eggs. Scale bar, 200 μm. Gr, germarium; O, oocyte; Pd, pedicel.

(B) Statistical summary of *L. striatellus* individuals with different ovarian development. Mean and SD were calculated from three independent experiments.

(C) Western blotting showing Vg protein levels in RSV-free and RSV-infected *L. striatellus* ovaries. Coomassie was used as a reference for sample loading.

(D) Flow cytometry staining to differentiate VgR^+ and VgR^- ovarian cells digested from RSV-free and RSV-infected *L. striatellus* ovaries.

(E) The number of VgR^+ cells corresponding to different fluorescence intensities in RSV-free and RSV-infected insects.

(F) Calculation of the percentages of the VgR^+ ovarian cells in RSV-free and RSV-infected insects.

(G) Western blotting showing VgR protein levels in the cytomembrane and cytoplasmic extracts of insect ovaries. The figures shown are representative of three independent biological replicates.

(H) Comparison of the number of eggs laid and nymphs emerged from RSV-free (healthy) and RSV-infected female insects. Mean and SD were calculated from three independent biological replicates. $*p < 0.05$; $**p < 0.01$; $***p < 0.001$; ns, not significant.

weaken or inactivate Rab1-GTP binding.[51–53] We therefore constructed corresponding LsRab1 mutants, $LsRab1^{S22N}$ and $LsRab1^{N121I}$. MST assays indicated that both recombinant mutant proteins have impaired GTP binding (Figures 5C and 5D). These results demonstrate the specific binding of LsRab1 with GDP and GTP.

Considering the identified interaction between RSV NP and LsRab1 (Figure 1), as well as the activated LsRab1-GTP molecular form for functioning, we investigated the tripartite interactions between LsRab1, GTP, and RSV NP. We measured the effects of NP binding to LsRab1 on subsequent GTP binding by pre-incubating RSV NP and LsRab1 before adding GTP. This

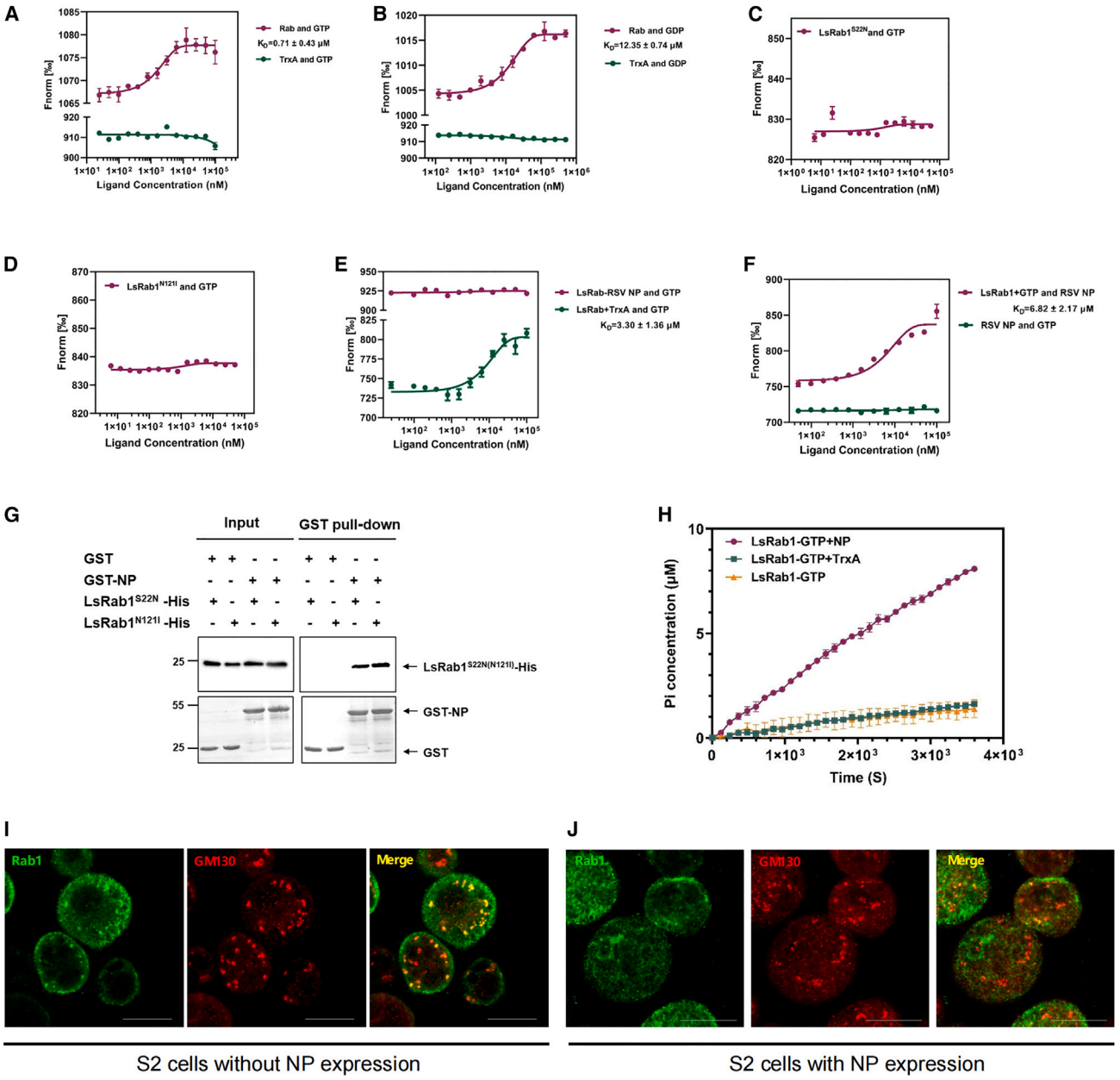

Figure 5. RSV NP-LsRab1 interaction inhibits LsRab1 activation

(A–D) MST assays showing the interaction between LsRab1 and GTP (A), LsRab1 and GDP (B), LsRab1^{S22N} and GTP (C), and LsRab1^{N121I} and GTP (D). TrxA was used as a negative control not binding to GTP, GDP, or LsRab1 proteins. Bars represent SD.

(E) MST to assay the molecular interaction between the LsRab1-NP complexes and GTP. LsRab1 and NP were preincubated to form a complex before GTP was added. Bars represent SD.

(F) MST to assay the molecular interaction between LsRab1-GTP and RSV NP. LsRab1 and GTP were preincubated to form a LsRab1-GTP complex before RSV NP was added. Bars represent SD.

(G) GST pull-down assays showing the interaction between RSV NP and the LsRab1 mutant proteins. GST was used as a negative control.

(H) The GTPase activity of LsRab1 was enhanced by RSV NP. The GTP hydrolysis activity of LsRab1 was tested in the presence or absence of RSV NP. Bars represent SD.

(I and J) Immunofluorescence assay showing the influence of RSV NP on Rab1 activity. (I) In the absence of RSV NP, Rab1 (green) colocalizes with the *cis*-Golgi marker GM130 (red) in *Drosophila* S2 cells. (J) In the presence of RSV NP, Rab1 fails to localize to the *cis*-Golgi marker GM130. Images are representative of three independent experiments. The scale bar represents 10 μm.

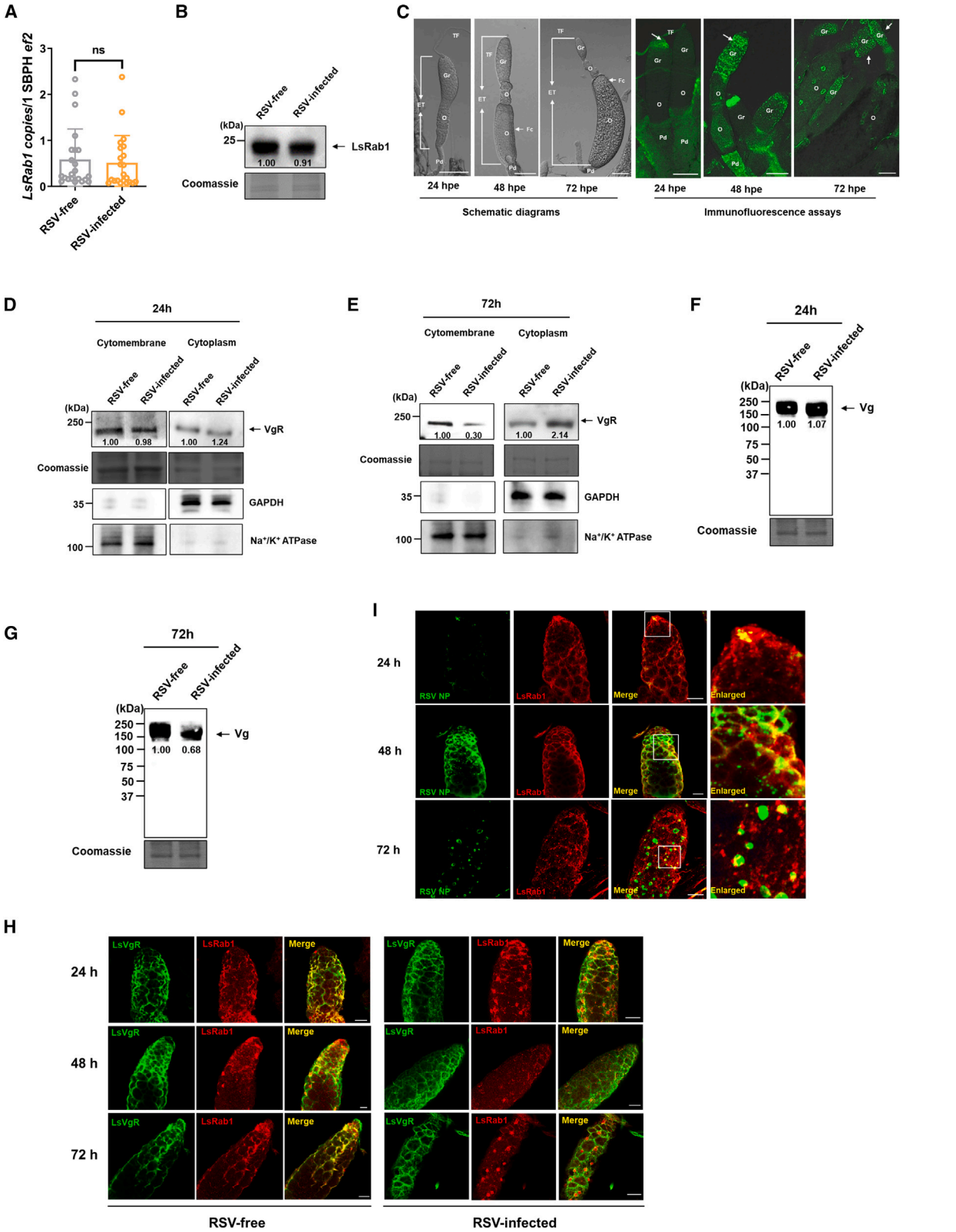

(legend on next page)

pre-treatment abolished the LsRab1's capability to subsequently bind GTP, indicating NP binding prevents GTP binding to LsRab1 (Figure 5E). We then tested whether RSV NP can bind to LsRab1 after pre-formation of LsRab1-GTP complexes. Results showed that RSV NP can still bind to pre-existing LsRab1-GTP complexes (Figure 5F). Using LsRab1^{S22N} and LsRab1^{N121I} mutants that do not bind GTP, we further confirmed that RSV NP could bind to LsRab1 in the absence of GTP binding (Figure 5G).

To investigate whether RSV NP binding to LsRab1-GTP influences intrinsic LsRab1 GTPase activity, we conducted an enzymatic assay. LsRab1 and GTP were preincubated to form LsRab1-GTP complexes, and then recombinant RSV NP or control TrxA protein was added. Measurement of GTP hydrolysis revealed that LsRab1 alone displays low intrinsic activity, but this was significantly enhanced by RSV NP binding (Figure 5H). To further confirm NP influence on Rab1 activity, we introduced RSV NP into *Drosophila* S2 cells for expression (Figure S6). In the absence of RSV NP, activated Rab1 proteins localized to the *cis*-Golgi, as indicated by co-localization with *cis*-Golgi marker GM130 (Figure 5I). Conversely, RSV NP expression prevented specific co-localization between Rab1 and GM130, suggesting RSV NP inhibits LsRab1 active form formation (Figure 5J).

Collectively, these results indicate two mechanisms by which RSV NP binds LsRab1 to inhibit its activation: (1) preventing GTP binding or (2) stimulating GTP hydrolysis of LsRab1-GTP complexes to decrease formation of the active GTP-bound form.

RSV infection reduces VgR membrane localization in an infection-severity-dependent manner

RSV NP dysfunctions LsRab1 *in vitro* and may inhibit LsRab1-mediated VgR trafficking *in vivo*. We first found that RSV infection did not alter *LsRab1* mRNA or protein levels (Figures 6A and 6B), supporting that RSV impacts LsRab1 activity rather than expression.

We next measured VgR membrane levels at different RSV infection time points to determine whether increasing ovarian infection severity would correlate with decreasing VgR localization to the cell surface. RSV RNPs were first detected in ovarian germarium at 24 hpe. By 48 hpe, RNPs occupied the entire germarium, occasionally extending into oocytes. At 72 hpe, RNPs had invaded oocytes and follicular cells (Figure 6C).

Compared to uninfected controls, we predicted much lower membrane VgR in infected females at 72 hpe. Indeed, western blotting showed negligible VgR impact at 24 hpe when few nurse cells were infected but significantly reduced surface VgR by 72 hpe during widespread infection (Figures 6D and 6E). Mirroring the VgR localization changes, continuous RSV invasion led to a gradual decrease in ovarian Vg accumulation over time (Figures 6F and 6G).

Confocal microscopy was employed to further validate the impact of RSV infection on VgR localization. In RSV-free ovaries, we observed a high degree of co-localization between VgR proteins and LsRab1, indicating proper secretion events (Figure 6H). In RSV-infected ovaries, as the infection progressed from 24 to 72 hpe, the co-localization rates between LsRab1 and VgR decreased significantly (Figure 6H). As a control, we observed that invading RSV co-localized with LsRab1, and the amount of co-localized LsRab1 proteins increased in proportion to RSV infection levels (Figure 6I). These confocal microscopy results further corroborated the in-ovary LsRab1-RSV NP interaction and its inhibitory effect on VgR localization.

Taken together, these results suggest that advancing RSV infection enables NP-LsRabl interaction, which inhibits LsRab1 activity, reducing VgR membrane localization in a manner dependent on infection severity and cell invasion.

DISCUSSION

Vector-borne plant viruses often exploit vector factors to facilitate vertical transmission. A common strategy involves hijacking the Vg-VgR transport pathway, a mechanism demonstrated in various vector-mediated pathogen transmissions.[17,22] However, the molecular events following viral entry into the ovaries remain largely unexplored. Our previous research has shown that RSV invades *L. striatellus* ovaries via the Vg-VgR pathway. In this study, we elucidated the molecular processes that occur after RSV initiates ovarian infection. Within the germarium nurse cells, RSV NP binds to LsRab1, disrupting its activity through two mechanisms. One is that NP binding to LsRab1 inhibits GTP binding. The other is that NP binding to LsRab1-GTP complexes activates GTPase activity, converting the active LsRab1-GTP to its inactive form. Through these mechanisms, LsRab1 loses its ability to promote VgR membrane localization, Vg uptake, and ovarian development. Consequently, this disruption impedes continued RSV cell entry (Figure 7).

Figure 6. RSV infection reduces VgR membrane localization in an infection-level-dependent manner

(A and B) RT-qPCR (A) and western blotting (B) showing that RSV infection does not affect *LsRab1* mRNA and protein levels. Mean and SD were calculated from three independent biological replicates. ns, not significant.

(C) Immunofluorescence assay to define different RSV infection levels in *L. striatellus* ovarioles over time. RSV was immunolabeled with rabbit anti-RSV antibody and stained with Alexa Fluor 488 (green). Arrows indicate RSV. Schematic diagrams of the ovarian structure of *L. striatellus* at 24, 48, and 72 hpe are shown on the left. TF, terminal filament; ET, egg tube; Gr, germarium; O, oocyte; Pd, pedicel; Fc, follicular cell. Scale bar, 100 μm.

(D and E) Western blotting showing VgR protein levels in the cytomembrane and cytoplasmic extracts of insect ovaries at 24 hpe (D) and 72 hpe (E). The transmembrane protein Na^+/K^+ ATPase and the cytoplasmic enzyme GAPDH are markers distinguishing the cytomembrane from the cytoplasm. Coomassie staining indicates the sample loading. The figures shown are representative of three independent biological replicates.

(F and G) Western blotting showing Vg protein levels in the cytomembrane and cytoplasmic extracts of insect ovaries at 24 hpe (F) and 72 hpe (G). The figures shown are representative of three independent biological replicates.

(H and I) Immunofluorescence assay showing the influence of RSV infection on VgR localization. (H) Co-localization between LsVgR (green) and LsRab1 (red) in RSV-free or RSV-infected ovaries. (I) Co-localization between RSV NP (green) and LsRab1 (red) in RSV-infected ovaries. Images are representative of three independent experiments. The scale bar represents 20 μm.

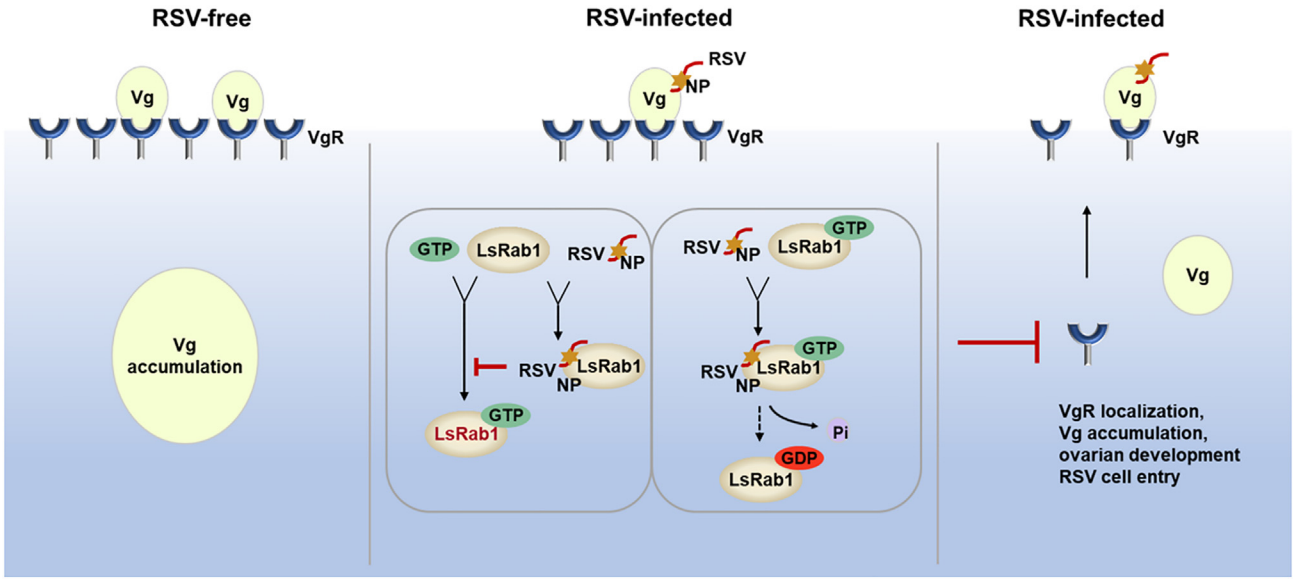

Figure 7. Proposed model for RSV NP-LsRab1 interaction regulating ovarian development and RSV entry

RSV invades *L. striatellus* ovaries via the Vg-VgR pathway. Inside ovarian cells, RSV NP binds LsRab1 to dysregulate its activity by two mechanisms: NP binding LsRab1 prevents GTP binding, and NP binding LsRab1-GTP complexes activates GTPase activity, converting active LsRab1-GTP to inactive form. Through both mechanisms, LsRab1 loses function in promoting VgR membrane localization, Vg uptake, ovarian development, and continued RSV cell entry.

Although both RSV infection and LsRab1 deficiency reduced VgR cell-surface localization and delayed ovarian development, the extent of effects differed. Under dsLsRab1 treatment, LsRab1 function was strongly inhibited in all ovarian cells. Consequently, minimal Vg entered cells via VgR (Figure 3B), thereby heavily inhibiting ovarian development (Figure 3A). In contrast, under natural RSV infection, the RSV-LsRab1 interaction limited VgR surface localization to a moderate level. Although viruliferous ovaries accumulate less Vg than healthy ones (Figure 4C), they still develop to maturity and produce RSV-infected eggs (Figures 4A and 4B). Unlike LsRab1 deficiency, which inhibits surface VgR in all ovarian cells, RSV NP dysfunctions LsRab1 only in infected cells. Therefore, at 24 hpe when few nurse cells are infected, surface VgR in RSV-infected ovaries is comparable to RSV-free ovaries (Figure 6D). However, at 72 hpe when most nurse cells and some oocytes have been infected, surface VgR in RSV-infected ovaries is significantly lower than in uninfected ovaries (Figure 6E). Confocal microscopy provides direct evidence for the infection-severity-dependent decrease in VgR localization. As RSV infection progresses, more LsRab1 colocalizes with RSV (Figure 6I), while less LsRab1 colocalizes with VgR for secretion (Figure 6H).

Our finding that RSV enters nurse cells via the VgR raises a question: if RSV then inhibits VgR membrane localization, does it inhibit its own continued infection? Two hypotheses may explain this self-limiting mechanism. One hypothesis is that these intricate molecular interplays reveal a delicate balancing act facilitating vertical transmission while allowing vector fertility. By partially blocking LsRab1-VgR trafficking, RSV maintains ovarian infection without severely impairing host reproduction. This feedback regulation of the RSV ovarian entry pathway may be a protection strategy for virus-infected individuals, ensuring survival rate of offspring. The other hypothesis is that by reducing membrane VgR in infected cells, more uninfected ovarian cells with abundant surface VgR have more opportunities to become targets for viral invasion. Therefore, viruses enter more ovarian cells to replicate and transmit, increasing the group infection ratio. The relationship between viruses and their arthropod vectors is complex, yet commonalities exist. Typically, successful interactions benefit both the virus and the insect, facilitating viral spread. In *L. striatellus*, previous studies revealed that RSV infection of the ovaries decreases insect fecundity, resulting in a reduced viruliferous population. Simultaneously, RSV infection shortens the nymphal stage duration, accelerating the production of viruliferous insects.[54] The mechanisms described in this study are also mutually beneficial for both the insect vector and the vectored virus. By limiting RSV infection levels to a certain extent, this RSV-SBPH interaction allows insects to survive while still enabling vertical virus transmission.

Although virus-vector relationships are generally more favorable than hostile pathogen-host interactions, viral infection still negatively impacts insects.[55] For example, infections by southern rice black-streaked dwarf virus, tomato yellow leaf curl geminivirus, and tomato spotted wilt virus reduce offspring numbers of vectors, likely by lowering egg production or hatching rates.[56–58] Previous studies investigating the impact of RSV infection on *L. striatellus* reproduction and development also revealed some adverse effects on SBPH, hindering the expansion of viruliferous populations.[59,60] This view is supported by systematic monitoring of SBPH viruliferous rates. In Jiangsu, China, following the occurrence of RSV infection in 2001, there was a rapid increase in the RSV-infected population from 2001 to

2003. The infection rate then remained at a high, stationary phase from 2003 to 2007, followed by a year-by-year decrease from 2007 to 2013.[60] Maintenance of the relatively friendly vector-virus relationships depends on delicate molecular interactions. Disruption of these interactions risks shifting toward more hostile relationships, as seen between leafhopper *Recilia dorsalis* and rice gall dwarf virus. Disturbances in the RNAi pathway led to excessive viral accumulation lethal to insects.[61]

Detailed mechanisms for viral vertical transmission are vital for rationally designing biological control strategies. While most research on viral vertical transmission focuses on overcoming ovarian barriers—the initial step in vertical transmission—this study first examines subsequent molecular events after viruses enter arthropod ovaries. Our findings add to the understanding of intricate virus-vector relationships, which can range from mutually beneficial to antagonistic. Disrupting these interactions can even push alliances toward hostility. A comprehensive picture of vertical infection pathways and virus-vector interactions will inform the rational design of targeted control measures. RSV's manipulation of the Vg-VgR pathway provides a new model for investigating vertical transmission of other medically and agriculturally important arboviruses.

Limitations of this study

Our investigation demonstrated the effects of LsRab1-RSV NP interaction on VgR intracellular trafficking through multiple lines of evidence. However, due to limitations in available cell lines, the most direct evidence remains to be obtained. Cellular-level imaging showing co-localization of LsRab1 and VgR on trafficking vesicles in the absence of RSV NP, and a reduction in VgR-related vesicles in the presence of RSV NP, would provide the most direct evidence.

For flow cytometry revealing the influence of RSV infection on VgR surface localization, we isolated ovarian cells from entire ovaries, which included nurse cells, follicle cells, oocytes, and other cell types. Isolating only nurse cells to measure VgR localization would have been ideal. However, the fragile nature of the tissue makes dissecting the germarium region alone technically challenging, presenting difficulties in obtaining intact germariums for analysis.

STAR★METHODS

Detailed methods are provided in the online version of this paper and include the following:

SUPPLEMENTAL INFORMATION

Supplemental information can be found online at https://doi.org/10.1016/j.celrep.2024.114571.

ACKNOWLEDGMENTS

This work is supported by the Major Program of the National Natural Science Foundation of China (32090013), the National Natural Science Foundation of China (32072385), and Youth Innovation Promotion Association CAS (2021084).

AUTHOR CONTRIBUTIONS

Conceptualization, Q.L., R.F., Y.H., and L.Z.; methodology, Q.L., Y.H., L.Z., and X.M.; formal analysis, Q.L. and X.M.; investigation, Q.L., X.M., Y.H., Z.S., Y.S., and Y.Z.; writing – original draft, Q.L. and Y.H.; writing – review & editing, Q.L., L.Z., Y.H., and X.M.; visualization, Q.L. and X.M.; supervision, R.F., Y.H., and L.Z.; project administration, Q.L., Y.H., and L.Z.; funding acquisition, Y.H. and L.Z.

DECLARATION OF INTERESTS

The authors declare no competing interests.

Received: February 27, 2024
Revised: June 23, 2024
Accepted: July 17, 2024
Published: August 1, 2024

REFERENCES

1. Jia, D., Chen, Q., Mao, Q., Zhang, X., Wu, W., Chen, H., Yu, X., Wang, Z., and Wei, T. (2018). Vector mediated transmission of persistently transmitted plant viruses. Curr. Opin. Virol. *28*, 127–132. https://doi.org/10.1016/j.coviro.2017.12.004.
2. Jia, D., Mao, Q., Chen, Y., Liu, Y., Chen, Q., Wu, W., Zhang, X., Chen, H., Li, Y., and Wei, T. (2017). Insect symbiotic bacteria harbour viral pathogens for transovarial transmission. Nat. Microbiol. *2*, 17025. https://doi.org/10.1038/nmicrobiol.2017.25.
3. Longdon, B., Wilfert, L., Obbard, D.J., and Jiggins, F.M. (2011). Rhabdoviruses in two species of *Drosophila*: vertical transmission and a recent sweep. Genetics *188*, 141–150. https://doi.org/10.1534/genetics.111.127696.
4. Chen, Q., Godfrey, K., Liu, J., Mao, Q., Kuo, Y.W., and Falk, B.W. (2019). A nonstructural protein responsible for viral spread of a novel insect reovirus provides a safe channel for biparental virus transmission to progeny. J. Virol. *93*, e00702–e00719. https://doi.org/10.1128/jvi.00702-19.
5. Abrahamian, P., Hammond, R.W., and Hammond, J. (2020). Plant virus-derived vectors: applications in agricultural and medical biotechnology. Annu. Rev. Virol. *7*, 513–535. https://doi.org/10.1146/annurev-virology-010720-054958.
6. Agboli, E., Leggewie, M., Altinli, M., and Schnettler, E. (2019). Mosquito-specific viruses—transmission and interaction. Viruses *11*, 873. https://doi.org/10.3390/v11090873.

7. Williams, T., Virto, C., Murillo, R., and Caballero, P. (2017). Covert infection of insects by baculoviruses. Front. Microbiol. *8*, 1337. https://doi.org/10.3389/fmicb.2017.01337.

8. Lequime, S., and Lambrechts, L. (2014). Vertical transmission of arboviruses in mosquitoes: a historical perspective. Infect. Genet. Evol. *28*, 681–690. https://doi.org/10.1016/j.meegid.2014.07.025.

9. Lequime, S., Paul, R.E., and Lambrechts, L. (2016). Determinants of arbovirus vertical transmission in mosquitoes. PLoS Pathog. *12*, e1005548. https://doi.org/10.1371/journal.ppat.1005548.

10. Xu, Y., Fu, S., Tao, X., and Zhou, X. (2021). Rice stripe virus: exploring molecular weapons in the arsenal of a negative-sense RNA virus. Annu. Rev. Phytopathol. *59*, 351–371. https://doi.org/10.1146/annurev-phyto-020620-113020.

11. Lu, G., Li, S., Zhou, C., Qian, X., Xiang, Q., Yang, T., Wu, J., Zhou, X., Zhou, Y., Ding, X.S., and Tao, X. (2019). Tenuivirus utilizes its glycoprotein as a helper component to overcome insect midgut barriers for its circulative and propagative transmission. PLoS Pathog. *15*, e1007655. https://doi.org/10.1371/journal.ppat.1007655.

12. Qin, F., Liu, W., Wu, N., Zhang, L., Zhang, Z., Zhou, X., and Wang, X. (2018). Invasion of midgut epithelial cells by a persistently transmitted virus is mediated by sugar transporter 6 in its insect vector. PLoS Pathog. *14*, e1007201. https://doi.org/10.1371/journal.ppat.1007201.

13. Chen, X., Yu, J., Wang, W., Lu, H., Kang, L., and Cui, F. (2020). A plant virus ensures viral stability in the hemolymph of vector insects through suppressing prophenoloxidase activation. mBio *11*, e01453-20. https://doi.org/10.1128/mBio.01453-20.

14. Lu, H., Zhu, J., Yu, J., Li, Q., Luo, L., and Cui, F. (2022). Key role of exportin 6 in exosome-mediated viral transmission from insect vectors to plants. Proc. Natl. Acad. Sci. USA *119*, e2207848119. https://doi.org/10.1073/pnas.2207848119.

15. Ma, Y., Lu, H., Wang, W., Zhu, J., Zhao, W., and Cui, F. (2021). Membrane association of importin α facilitates viral entry into salivary gland cells of vector insects. Proc. Natl. Acad. Sci. USA *118*, e2103393118. https://doi.org/10.1073/pnas.2103393118.

16. Huang, H.J., Wang, Y.Z., Li, L.L., Lu, H.B., Lu, J.B., Wang, X., Ye, Z.X., Zhang, Z.L., He, Y.J., Lu, G., et al. (2023). Planthopper salivary sheath protein LsSP1 contributes to manipulation of rice plant defenses. Nat. Commun. *14*, 737. https://doi.org/10.1038/s41467-023-36403-5.

17. Huo, Y., Liu, W., Zhang, F., Chen, X., Li, L., Liu, Q., Zhou, Y., Wei, T., Fang, R., and Wang, X. (2014). Transovarial transmission of a plant virus is mediated by vitellogenin of its insect vector. PLoS Pathog. *10*, e1003949. https://doi.org/10.1371/journal.ppat.1003949.

18. Huo, Y., Yu, Y., Liu, Q., Liu, D., Zhang, M., Liang, J., Chen, X., Zhang, L., and Fang, R. (2019). Rice stripe virus hitchhikes the vector insect vitellogenin ligand-receptor pathway for ovary entry. Philos. Trans. R. Soc. Lond. B Biol. Sci. *374*, 20180312. https://doi.org/10.1098/rstb.2018.0312.

19. Lefkowitz, E.J., Dempsey, D.M., Hendrickson, R.C., Orton, R.J., Siddell, S.G., and Smith, D.B. (2018). Virus taxonomy: the database of the International Committee on Taxonomy of Viruses (ICTV). Nucleic Acids Res. *46*, D708–D717. https://doi.org/10.1093/nar/gkx932.

20. Toriyama, S., Takahashi, M., Sano, Y., Shimizu, T., and Ishihama, A. (1994). Nucleotide sequence of RNA 1, the largest genomic segment of rice stripe virus, the prototype of the tenuiviruses. J. Gen. Virol. *75*, 3569–3579. https://doi.org/10.1099/0022-1317-75-12-3569.

21. Falk, B.W., and Tsai, J.H. (1998). Biology and molecular biology of viruses in the genus Tenuivirus. Annu. Rev. Phytopathol. *36*, 139–163. https://doi.org/10.1146/annurev.phyto.36.1.139.

22. Huo, Y., Yu, Y., Chen, L., Li, Q., Zhang, M., Song, Z., Chen, X., Fang, R., and Zhang, L. (2018). Insect tissue-specific vitellogenin facilitates transmission of plant virus. PLoS Pathog. *14*, e1006909. https://doi.org/10.1371/journal.ppat.1006909.

23. Raikhel, A.S., and Dhadialla, T.S. (1992). Accumulation of yolk proteins in insect oocytes. Annu. Rev. Entomol. *37*, 217–251. https://doi.org/10.1146/annurev.en.37.010192.001245.

24. Sappington, T.W., and Raikhel, A.S. (1998). Molecular characteristics of insect vitellogenins and vitellogenin receptors. Insect Biochem. Mol. Biol. *28*, 277–300. https://doi.org/10.1016/s0965-1748(97)00110-0.

25. Wei, J., He, Y.Z., Guo, Q., Guo, T., Liu, Y.Q., Zhou, X.P., Liu, S.S., and Wang, X.W. (2017). Vector development and vitellogenin determine the transovarial transmission of begomoviruses. Proc. Natl. Acad. Sci. USA *114*, 6746–6751. https://doi.org/10.1073/pnas.1701720114.

26. Brasset, E., Taddei, A.R., Arnaud, F., Faye, B., Fausto, A.M., Mazzini, M., Giorgi, F., and Vaury, C. (2006). Viral particles of the endogenous retrovirus ZAM from Drosophila melanogaster use a pre-existing endosome/exosome pathway for transfer to the oocyte. Retrovirology *3*, 25. https://doi.org/10.1186/1742-4690-3-25.

27. Homma, Y., Hiragi, S., and Fukuda, M. (2021). Rab family of small GTPases: an updated view on their regulation and functions. FEBS J. *288*, 36–55. https://doi.org/10.1111/febs.15453.

28. Stenmark, H. (2009). Rab GTPases as coordinators of vesicle traffic. Nat. Rev. Mol. Cell Biol. *10*, 513–525. https://doi.org/10.1038/nrm2728.

29. Plutner, H., Cox, A.D., Pind, S., Khosravi-Far, R., Bourne, J.R., Schwaninger, R., Der, C.J., and Balch, W.E. (1991). Rab1b regulates vesicular transport between the endoplasmic reticulum and successive Golgi compartments. J. Cell Biol. *115*, 31–43. https://doi.org/10.1083/jcb.115.1.31.

30. Spang, A. (2013). Retrograde traffic from the Golgi to the endoplasmic reticulum. Cold Spring Harbor Perspect. Biol. *5*, a013391. https://doi.org/10.1101/cshperspect.a013391.

31. Szul, T., and Sztul, E. (2011). COPII and COPI traffic at the ER-Golgi interface. Physiology *26*, 348–364. https://doi.org/10.1152/physiol.00017.2011.

32. Wang, B., Stanford, K.R., and Kundu, M. (2020). ER-to-Golgi Trafficking and Its Implication in Neurological Diseases. Cells *9*, 408. https://doi.org/10.3390/cells9020408.

33. Lord, C., Ferro-Novick, S., and Miller, E.A. (2013). The highly conserved COPII coat complex sorts cargo from the endoplasmic reticulum and targets it to the golgi. Cold Spring Harbor Perspect. Biol. *5*, a013367. https://doi.org/10.1101/cshperspect.a013367.

34. Bär, S., Rommelaere, J., and Nüesch, J.P.F. (2013). Vesicular transport of progeny parvovirus particles through ER and Golgi regulates maturation and cytolysis. PLoS Pathog. *9*, e1003605. https://doi.org/10.1371/journal.ppat.1003605.

35. Li, G., and Marlin, M.C. (2015). Rab family of GTPases. Methods Mol. Biol. *1298*, 1–15. https://doi.org/10.1007/978-1-4939-2569-8_1.

36. Raza, S., Alvisi, G., Shahin, F., Husain, U., Rabbani, M., Yaqub, T., Anjum, A.A., Sheikh, A.A., Nawaz, M., and Ali, M.A. (2018). Role of Rab GTPases in HSV-1 infection: molecular understanding of viral maturation and egress. Microb. Pathog. *118*, 146–153. https://doi.org/10.1016/j.micpath.2018.03.028.

37. Zhuang, X., Adipietro, K.A., Datta, S., Northup, J.K., and Ray, K. (2010). Rab1 small GTP-binding protein regulates cell surface trafficking of the human calcium-sensing receptor. Endocrinology *151*, 5114–5123. https://doi.org/10.1210/en.2010-0422.

38. Zhang, X., Wang, G., Dupré, D.J., Feng, Y., Robitaille, M., Lazartigues, E., Feng, Y.H., Hébert, T.E., and Wu, G. (2009). Rab1 GTPase and dimerization in the cell surface expression of angiotensin II type 2 receptor. J. Pharmacol. Exp. Therapeut. *330*, 109–117. https://doi.org/10.1124/jpet.109.153460.

39. Filipeanu, C.M., Zhou, F., Fugetta, E.K., and Wu, G. (2006). Differential regulation of the cell-surface targeting and function of beta- and alpha1-adrenergic receptors by Rab1 GTPase in cardiac myocytes. Mol. Pharmacol. *69*, 1571–1578. https://doi.org/10.1124/mol.105.019984.

40. Castellano, F., Wilson, A.L., and Maltese, W.A. (1995). Intracellular transport and maturation of nascent low density lipoprotein receptor is blocked

by mutation in the Ras-related GTP-binding protein. J. Recept. Signal Transduct. Res. *15*, 847–862. https://doi.org/10.3109/10799899509049861.

41. Zhang, Y., Wang, L., Lv, Y., Jiang, C., Wu, G., Dull, R.O., Minshall, R.D., Malik, A.B., and Hu, G. (2019). The GTPase Rab1 is required for NLRP3 inflammasome activation and inflammatory lung injury. J. Immunol. *202*, 194–206. https://doi.org/10.4049/jimmunol.1800777.
42. Wu, G. (2008). Regulation of the trafficking and function of G protein-coupled receptors by Rab1 GTPase in cardiomyocytes. Methods Enzymol. *438*, 227–238. https://doi.org/10.1016/s0076-6879(07)38016-6.
43. Seachrist, J.L., Laporte, S.A., Dale, L.B., Babwah, A.V., Caron, M.G., Anborgh, P.H., and Ferguson, S.S.G. (2002). Rab5 association with the angiotensin II type 1A receptor promotes Rab5 GTP binding and vesicular fusion. J. Biol. Chem. *277*, 679–685. https://doi.org/10.1074/jbc.M109022200.
44. Nachmias, D., Sklan, E.H., Ehrlich, M., and Bacharach, E. (2012). Human immunodeficiency virus type 1 envelope proteins traffic toward virion assembly sites via a TBC1D20/Rab1-regulated pathway. Retrovirology *9*, 7. https://doi.org/10.1186/1742-4690-9-7.
45. Zenner, H.L., Yoshimura, S.I., Barr, F.A., and Crump, C.M. (2011). Analysis of Rab GTPase-activating proteins indicates that Rab1a/b and Rab43 are important for herpes simplex virus 1 secondary envelopment. J. Virol. *85*, 8012–8021. https://doi.org/10.1128/jvi.00500-11.
46. Yamayoshi, S., Neumann, G., and Kawaoka, Y. (2010). Role of the GTPase Rab1b in ebolavirus particle formation. J. Virol. *84*, 4816–4820. https://doi.org/10.1128/jvi.00010-10.
47. Takacs, C.N., Andreo, U., Dao Thi, V.L., Wu, X., Gleason, C.E., Itano, M.S., Spitz-Becker, G.S., Belote, R.L., Hedin, B.R., Scull, M.A., et al. (2017). Differential regulation of lipoprotein and Hepatitis C Virus secretion by Rab1b. Cell Rep. *21*, 431–441. https://doi.org/10.1016/j.celrep.2017.09.053.
48. Zhu, J., Jiang, F., Wang, X., Yang, P., Bao, Y., Zhao, W., Wang, W., Lu, H., Wang, Q., Cui, N., et al. (2017). Genome sequence of the small brown planthopper, *Laodelphax striatellus*. GigaScience *6*, 1–12. https://doi.org/10.1093/gigascience/gix109.
49. Jones, S., Newman, C., Liu, F., and Segev, N. (2000). The TRAPP complex is a nucleotide exchanger for Ypt1 and Ypt31/32. Mol. Biol. Cell *11*, 4403–4411. https://doi.org/10.1091/mbc.11.12.4403.
50. Kim, Y.G., Raunser, S., Munger, C., Wagner, J., Song, Y.L., Cygler, M., Walz, T., Oh, B.H., and Sacher, M. (2006). The architecture of the multisubunit TRAPP I complex suggests a model for vesicle tethering. Cell *127*, 817–830. https://doi.org/10.1016/j.cell.2006.09.029.
51. Allan, B.B., Moyer, B.D., and Balch, W.E. (2000). Rab1 recruitment of p115 into a cis-SNARE complex: programming budding COPII vesicles for fusion. Science *289*, 444–448. https://doi.org/10.1126/science.289.5478.444.
52. Bahl, S., Parashar, S., Malhotra, H., Raje, M., and Mukhopadhyay, A. (2015). Functional Characterization of Monomeric GTPase Rab1 in the Secretory Pathway of Leishmania. J. Biol. Chem. *290*, 29993–30005. https://doi.org/10.1074/jbc.M115.670018.
53. Wilson, B.S., Nuoffer, C., Meinkoth, J.L., McCaffery, M., Feramisco, J.R., Balch, W.E., and Farquhar, M.G. (1994). A Rab1 mutant affecting guanine nucleotide exchange promotes disassembly of the Golgi apparatus. J. Cell Biol. *125*, 557–571. https://doi.org/10.1083/jcb.125.3.557.
54. Li, S., Wang, S., Wang, X., Li, X., Zi, J., Ge, S., Cheng, Z., Zhou, T., Ji, Y., Deng, J., et al. (2015). Rice stripe virus affects the viability of its vector offspring by changing developmental gene expression in embryos. Sci. Rep. *5*, 7883. https://doi.org/10.1038/srep07883.
55. Perlmutter, J.I., and Bordenstein, S.R. (2020). Microorganisms in the reproductive tissues of arthropods. Nat. Rev. Microbiol. *18*, 97–111. https://doi.org/10.1038/s41579-019-0309-z.
56. Rubinstein, G., and Czosnek, H. (1997). Long-term association of tomato yellow leaf curl virus with its whitefly vector Bemisia tabaci: effect on the insect transmission capacity, longevity and fecundity. J. Gen. Virol. *78*, 2683–2689. https://doi.org/10.1099/0022-1317-78-10-2683.
57. Ogada, P.A., Maiss, E., and Poehling, H.-M. (2013). Influence of tomato spotted wilt virus on performance and behaviour of western flower thrips (*Frankliniella occidentalis*). J. Appl. Entomol. *137*, 488–498. https://doi.org/10.1111/jen.12023.
58. Xu, H., He, X., Zheng, X., Yang, Y., Tian, J., and Lu, Z. (2014). Southern rice black-streaked dwarf virus (SRBSDV) directly affects the feeding and reproduction behavior of its vector, *Sogatella furcifera* (Horváth) (Hemiptera: Delphacidae). Virol. J. *11*, 55. https://doi.org/10.1186/1743-422X-11-55.
59. Wan, G., Jiang, S., Wang, W., Li, G., Tao, X., Pan, W., Sword, G.A., and Chen, F. (2015). Rice stripe virus counters reduced fecundity in its insect vector by modifying insect physiology, primary endosymbionts and feeding behavior. Sci. Rep. *5*, 12527. https://doi.org/10.1038/srep12527.
60. He, K., Guo, J.M., Li, F., Lin, K.J., and Wang, G.R. (2018). Impact of the Rice stripe virus (RSV) on the biological, physiological and biochemical characteristics of the small brown planthopper, *Laodelphax striatellus* (Hemiptera: Delphacidae). Chin. J. Appl. Entomol. *55*, 87–95. https://doi.org/10.7679/j.issn.2095-1353.2018.014.
61. Lan, H., Wang, H., Chen, Q., Chen, H., Jia, D., Mao, Q., and Wei, T. (2016). Small interfering RNA pathway modulates persistent infection of a plant virus in its insect vector. Sci. Rep. *6*, 20699. https://doi.org/10.1038/srep20699.
62. Pereira-Leal, J.B., and Seabra, M.C. (2001). Evolution of the Rab family of small GTP-binding proteins. J. Mol. Biol. *313*, 889–901. https://doi.org/10.1006/jmbi.2001.5072.
63. Saitou, N., and Nei, M. (1987). The neighbor-joining method: a new method for reconstructing phylogenetic trees. Mol. Biol. Evol. *4*, 406–425. https://doi.org/10.1093/oxfordjournals.molbev.a040454.
64. Tamura, K., Stecher, G., Peterson, D., Filipski, A., and Kumar, S. (2013). MEGA6: Molecular Evolutionary Genetics Analysis Version 6.0. Mol. Biol. Evol. *30*, 2725–2729. https://doi.org/10.1093/molbev/mst197.
65. Sala, D., Engelberger, F., McHaourab, H.S., and Meiler, J. (2023). Modeling conformational states of proteins with AlphaFold. Curr. Opin. Struct. Biol. *81*, 102645. https://doi.org/10.1016/j.sbi.2023.102645.

STAR★METHODS

KEY RESOURCES TABLE

REAGENT or RESOURCE	SOURCE	IDENTIFIER
Antibodies		
Mouse monoclonal anti-His	TIANGEN	Cat# AB102-02; RRID: AB_2728089
Mouse monoclonal anti-GST	Abmart	Cat# M20025; RRID: AB_2936260
Rabbit polyclonal anti-GM130	Abcam	Cat# ab30637; RRID: AB_732675
Rabbit polyclonal anti-Vg	Huo et al.[22]	N/A
Mouse polyclonal anti-VgR	This paper	N/A
Mouse monoclonal anti-RSV NP	Huo et al.[17]	N/A
Rabbit polyclonal anti-RSV NP	Huo et al.[17]	N/A
Mouse polyclonal anti-LsRab1	This paper	N/A
Rabbit polyclonal anti-Rab1	Proteintech	Cat# 11671-1-AP; RRID: AB_2173437
Rabbit polyclonal anti-GAPDH	Abclonal	Cat# A19056; RRID: AB_2862549
Rabbit polyclonal anti-Na^+/K^+ -ATPase	Cell Signaling Technology	Cat# 3010; RRID: AB_2060983
Alexa Fluor 488-conjugated goat anti-mouse	ThermoFisher	Cat# A11029; RRID: AB_2534088
Alexa Fluor 568-conjugated goat anti-mouse	ThermoFisher	Cat# A11031; RRID: AB_144696
Alexa Fluor 568-conjugated goat anti-Rabbit	ThermoFisher	Cat# A11036; RRID: AB_10563566
Alexa Fluor 488-conjugated goat anti-Rabbit	ThermoFisher	Cat# A11034; RRID: AB_2576217
Bacterial and virus strains		
Escherichia coli (BL21)	TransGen Biotech	Cat# CD601
Escherichia coli (DH5α)	Tsingke	Cat# TSC-C14
Chemicals, peptides, and recombinant proteins		
ProLong™ Gold Antifade Mountant with DAPI	Invitrogen	Cat# P36941
GTP	Invitrogen	Cat# AM8130G
GDP	Sigma	Cat# G7127
Elastase	Worthington	Cat# LS002292
Collagenase	Thermo	Cat# 17100017
Glutathione Sepharose beads	GE	Cat# 17-3712-02
iQ SYBR Green Supermix	BIO-RAD	Cat# 1708882
PMSF	Thermo	Cat# 36978
Cell dissociation buffer	Thermo Fisher	Cat# 13151014
Critical commercial assays		
RNeasy Mini Kit	QIAGEN	Cat# 74104
ER protein extraction kit	BestBio	Cat# BB-31454-1
Golgi protein extraction kit	BestBio	Cat# BB-3604-1
Monolith NT Protein Labeling Kit RED-NHS	Nanotemper	Cat# MO-L001
T7 RiboMAX™ Express RNAi System	Promega	Cat# P1700
EnzChek phosphate assay kit	Invitrogen	Cat# E6646
iScript cDNA Synthesis Kit	Bio-Rad	Cat# 1708891
Co-Immunocoprecipitation kit	Thermo Fisher	Cat# 26149
Experimental models: Cell lines		
S2	ATCC	Cat# CRL-1963, RRID:CVCL_Z232
Experimental models: Organisms/strains		
Laodelphax striatellus	Reared in greenhouse	N/A
Oligonucleotides		
The complete list of oligonucleotides are presented in Table S5	This paper	N/A

(*Continued on next page*)

Continued

REAGENT or RESOURCE	SOURCE	IDENTIFIER
Recombinant DNA		
pET30a-LsRab1-His	This paper	N/A
pET30a-LsRab1^{N121I}-His	This paper	N/A
pET30a-LsRab1^{S22N}-His	This paper	N/A
pET30a-NLsRab1-His	This paper	N/A
pET30a-CLsRab1-His	This paper	N/A
pGEX-3X-GST-NP	This paper	N/A
pMT-V5-His-NP	This paper	N/A
Software and algorithms		
ImageJ	NIH	https://imagej.net.
GraphPad Prism 9	GraphPad	https://www.graphpad.com/
CytExpert software	Beckman	https://www.mybeckman.cn/
Mo Affinity Analysis Software	Nanotemper	https://shop.nanotempertech.com/
LAS X	Leica Microsystems	https://www.leica-microsystems.com.cn/
Mascot	Matrix Science	https://www.matrixscience.com/
AlphaFold2	DeepMind	https://colab.research.google.com/github/deepmind/alphafold/
MEGA6	Tamura et al.[64]	https://www.megasoftware.net/
Other		
Filter	Corning	Cat# 352350
96-well half-area microplates	Corning	Cat# 3695
Mass spectrometry	Thermo	Orbitrap Fusion Lumos Tribrid
Monolith NT.115 Microscale Thermophoresis	Nanotemper	MST-nanotemper
laser scanning confocal microscope	Leica	Leica SP8
Nanoject II Programmable Nanoliter injector	World Precision Instruments	Nanoliter 2000
Gallios flow cytometer	Beckman	Cytoflex LX
microplate spectrometer	Switzerland TECAN	Infinite M200 Pro

RESOURCE AVAILABILITY

Lead contact

Further information and requests for resources and reagents should be directed to and will be fulfilled by the lead contact, Lili Zhang (zhangll@im.ac.cn).

Materials availability

Newly generated materials from this study will be available upon reasonable request.

Data and code availability

- All data supporting the findings of this study are available from the lead contact upon reasonable request.
- Any additional information required to reanalyze the data reported in this paper is available from the lead contact upon request.
- This paper does not report original code.

EXPERIMENTAL MODEL AND STUDY PARTICIPANT DETAILS

RSV-free and RSV-infected *L. striatellus* individuals were originally captured in Jiangsu Province, China, and were maintained in our laboratory. All plants used for *L. striatellus* rearing were grown inside a growth incubator at 25°C under a 16-h light/8-h dark photoperiod.[17] To ensure high infection rate in offspring, RSV-infected female imagoes were cultured separately. Then, 15% of their offspring were tested for RSV infection by dot ELISA using RSV-specific olyclonal rabbit antibodies.

METHOD DETAILS

Tissue collection

Insect dissection and tissue collection were performed following previously described procedures.[22] Insects were anesthetized on ice for 10–20 min, then the abdominal pouch was torn open in a drop of water. The ovaries or midgut were expelled and placed in clean PBS buffer inside the microtubes. If the developmental stage of the ovary is to be determined, the dissected ovary is placed on a glass slide, covered with gold antifade (Invitrogen, USA) for microscope observation. For hemolymph isolation, the forelegs were severed at the coxa-trochanter joint with forceps. Hemolymph is expelled and drawn to clean forceps tips. Use forceps to collect as much fat body as possible, i.e., the loose white oily substance, and placed in PBS buffer.

RT-qPCR

For quantitative analysis of gene expression in SBPH tissues, total RNA was extracted from dissected tissues using RNeasy Mini Kit (QIAGEN, Germany) according to the manufacturer's protocol. Reverse transcriptional PCR (Bio-rad) and SYBR-Green-based qPCR were performed according to the protocols provided by the manufacturer (Bio-rad, USA). *L. striatellus* elongation factor 2 (EF2) was amplified as an internal control for the loading of cDNA isolated from different samples. Water was used as a negative control. Primer pairs used for PCR amplification are listed in Table S5.

Antibody preparation

The rabbit anti-Vg antibodies designated as Ab67K2 against the Vg peptide YKNPGEAPELR and the mouse anti-VgR antibodies against the VgR peptide QKCNNLVGSYRCSCDR were prepared before in our lab.[22,60] This VgR antibody was used in the flow cytometry staining and western blotting. The RSV-specific antibody for immunofluorescence assay was produced using RSV ribonucleoproteins (RNPs) as antigen to immunize rabbit, and the RSV RNPs were purified from RSV-infected rice plants. The anti-RSV RNP monoclonal antibodies provided by Dr. Xueping Zhou (Institute of Biotechnology, Zhejiang University) were used in the Co-IP assay. The specificity of the anti-RSV RNP antibody has been validated in our previous study.[17] Additionally, we have detected RSV NP in the ovaries of infected and RSV-free *L.striatellus*, respectively, using this RSV RNP antibody by western blot, further demonstrating its specificity (Figure 1A). To prepare LsRab1-specific antibodies for immunofluorescence assay and western blotting, the full-length *LsRab1* gene was PCR amplified using primers LsRab1-F/LsRab1-R (Table S5) and was cloned into pET30a for expression. The purified proteins contain a C-terminal 6*His tag, which were used to immunize mouse to produce antibodies.

Western blotting analysis

Western blotting was performed to measure the distribution of Vg and VgR in different *L. striatellus* tissues, or the distribution of VgR and LsRab1 in different organelles in ovary. To determine the tissue distribution, tissues were dissected from the insects. Hemolymph or ovaries from 30 insects were placed in 200 μL of PBS buffer to boil in SDS-PAGE loading buffer. SDS-PAGE was run to determine the protein concentration, and then same amounts of total proteins were fractionated by SDS-PAGE and were hybridized with Vg- or VgR-specific antibodies.

To determine the distribution of VgR proteins in cytoplasm and cytomembrane, ovaries were dissected from 50 RSV-free or RSV-infected females at 48 hpe and lysed in 200 μL of cell lysate (1 mM KCl, 5 mM NaCl, 3 mM MgCl, 50 mM HEPES, 1 mM DTT, 0.5 μg Lenpeptin, 20 μM PMSF, 1 mM EDTA, pH 7.4) for 30 min at 4°C. After centrifugation at 12,000 rpm for 10 min at 4°C, the supernatant was collected as the cytoplasmic protein extract. The pellet was resuspended in 200 μL of PBS buffer containing 20 μM PMSF to obtain the cytomembrane protein extract. Equal volumes of cytoplasm and cytomembrane protein extracts were fractionated by SDS-PAGE and hybridized with VgR-specific antibodies. The transmembrane protein Na^+/K^+ ATPase and the cytoplasmic enzyme GAPDH were selected as markers to distinguish the cytomembrane from the cytoplasm.

Co-immunoprecipitation (Co-IP) assay

The Co-IP assay was carried out according to the manufacturer's instructions (Thermo Fisher Scientific, USA). Initially, 50 ng of RSV RNP-specific mouse monoclonal antibodies were immobilized to the coupling resin and incubated at room temperature for 90 min. Approximately 50 ovaries dissected from RSV-infected at 48 hpe were homogenized in PBS buffer, while ovaries from RSV-free females served as a negative control. Ice-cold IP lysis buffer was added to the tissue homogenate and incubated on ice for 30 min. The lysate was centrifuged at 13,000g for 10 min to pellet the tissue and cell debris. The supernatant was incubated with the antibody-immobilized resins for 3 h at 4°C. The resin was washed three times with wash buffer. Subsequently, 50 μL of elution buffer was added and incubated at room temperature for 10 min. The elution process was performed three times in total, yielding E1, E2, and E3. E1-E3 containing ovarian proteins were analyzed by mass spectrometry (Mass spectrometry and functional omics platform, Institute of Microbiology, Chinese Academy of Sciences). All IP-MS samples digested with enzyme trypsin were confidently identified using Mascot (Matrix Science, London, UK; version 2.8.0). Mascot was set up to search the *L. striatellus* protein database download from NCBI. The search was performed with a fragment ion mass tolerance of 0.02 Da and a parent ion tolerance of 10.0 ppm. To confirm the Co-IP results, the resins were directly running SDS-PAGE for western blotting with mouse anti-LsRab1 antibody.

Microscale thermophoresis (MST) assays

MST assays were performed to detect the interactions between LsRab1 proteins and GTP/GDP, LsRab1 and RSV NP, the tripartite LsRab1-NP-GTP interactions, and LsRab1 and VgR-CP. For these assays, full-length LsRab1 or the mutant proteins, RSV NP, and VgR-CP (amino acids 1797–1927) were recombinantly expressed in *E. coli* with C-terminal His-tags. As a relevant control for His-tagged fusion proteins, TrxA co-expressed with a His-tag was expressed as a control protein.

To determine the LsRab1s-GTP/GDP and LsRab1s-NP interactions, 10 μM purified LsRab1s was labeled with a Monolith NT Protein Labeling Kit RED-NHS (Nano Temper Technologies GMBH, Germany) using red fluorescent dye NT-647 N-hydroxysuccinimide (amine-reactive) according to the manufacturer's instructions. The binding assays were performed on a Monolith NT.115 Microscale Thermophoresis instrument (Nano Temper Technologies GMBH, Germany) using standardly treated capillaries. The labeled protein LsRab1s was added to serially diluted protein reaction volumes of GTP, GDP, NP, or TrxA at an initial concentration of 200 μM (NP and TrxA concentration were 100 μM) containing 0.5% (v/v) Tween 20. The KD Fit function of NanoTemper Analysis software version 1.2.214.1 was used for curve fitting and calculation of the value of the dissociation constant (K_D). To determine the LsRab1- VgR-CP interaction, the labeled LsRab1 was added to serially diluted protein reaction volumes of VgR-CP.

To determine whether NP binding to LsRab1 influence the interaction between LsRab1 and GTP, 10 μM RED-NHS-labeled LsRab1 was pre-incubated with 10 μM NP for 1 h at room temperature. 10 μM TrxA was used as a negative control to pre-incubate with the labeled LsRab1. The labeled LsRab1-NP/TrxA mixture was added to serially diluted protein reaction volumes of GTP at an initial concentration of 200 μM containing 0.5% (v/v) Tween 20.

To determine whether LsRab1-GTP complex could still bind NP, 10 μM RED-NHS-labeled LsRab1 was pre-incubated with 10 μM GTP for 1 h at room temperature. The labeled LsRab1-GTP mixture was added to serially diluted protein reaction volumes of NP at an initial concentration of 100 μM containing 0.5% (v/v) Tween 20. As a negative control, the NP-GTP interaction was measured, in which 10 μM purified NP was labeled with RED-NHS.

GST pull-down assay

GST pull-down assay was performed to determine the interaction between LsRab1 and RSV NP. The full-length NP was expressed in *E. coli* as a GST-fusion protein (GST-NP), and LsRab1 was expressed with a C-terminal His-tag. GST was used as a negative control. The GST-NP or GST was bound to glutathione Sepharose beads (GE, USA) for 3 h at 4°C; the mixtures were centrifuged for 5 min at 100 x g and the supernatants were discarded; the LsRab-His was added to the beads and incubated for 2 h at 4°C. After being centrifuged and washed five times, the bead-bound proteins were separated by SDS-PAGE gel electrophoresis and detected by western blotting with antibodies against his-tag (TIANGEN, Beijing, China) and GST (Abmart, Shanghai, China).

Immunofluorescence microscopy

The ovaries dissected from RSV-infected female *L. striatellus* at 48 hpe were fixed in 4% paraformaldehyde in PBS for 1 h at room temperature. The fixed ovaries were incubated in an osmotic buffer (2% Triton v/v in PBS) for 4 h at room temperature, incubated with rabbit anti-RSV and mouse anti-LsRab1 antibodies for 1 h at room temperature, and then incubated with Alexa Fluor 488-conjugated goat anti-rabbit antibody and Alexa Fluor 568-conjugated goat anti-mouse antibody (Invitrogen, USA) for 1 h. The samples were observed with a laser scanning confocal microscope (Leica TCS SP8) and the images were saved by Leica LAS AF Lite.

RNA interference

LsRab1-specific gene fragment was PCR amplified with the primer pair dsLsRab1-F/dsLsRab1-R (Table S5). DsRNA was synthesized using a commercial kit (T7 RiboMAX Express RNAi System, Promega) and purified by phenol:chloroform extraction and isopropanol precipitation. The 5th instar nymphs were microinjected with 23.8 nL of dsRNA at 1 ng/nL for gene silencing. Microinjection was performed using a glass needle through a Nanoliter 2000 (World Precision Instruments, Sarasota, FL, USA). gfp dsRNA, which was used as a negative control, was synthesized and microinjected following the same protocol. The dsRNA-treated insects were allowed to emerge into adults and the newly emerged females were transferred to RSV-free plants to feed for 48 h. The silencing efficiency of *LsRab1* was measured at 48 hpe.

Flow cytometry

Flow cytometry was used to analyze the VgR^+-cell levels in the ovarian cell samples. 30 ovaries were dissected from the RSV-free, RSV-infected, *dsRab1*-treated, or the *dsgfp*-treated 48-hpe females and were suspended in 200 μL of cell dissociation buffer (Thermo Fisher, USA). Cells were dissociated with 4 mg/mL elastase (Worthington, USA) and 2.5 mg/mL collagenase (Thermo Fisher, USA) at room temperature with continuous gentle shaking for 15–20 min. After passing through a 70 μm filter (Corning, USA), the filtered cells were collected by centrifugation at 5,000 x g for 1 min. The cells were washed in PBS and then sequentially incubated with PBS +0.04% BSA, mouse anti-VgR antibodies, and Alexa-fluor 488-conjugated goat anti-mouse antibody. After washed with PBS buffer, the cells were counted under a microscope. A minimum of 10^6 cells/ml was acquired. Flow cytometry was performed on a Gallios flow cytometer (Beckman Cytoflex LX, USA), and the data were analyzed using the CytExpert software. A minimum of 10,000 cells/event was analyzed.

GTPase activity assay

To assess the GTPase activity of LsRab1, an EnzChek phosphate assay kit (Invitrogen, USA) was used following the manufacturer's instructions.[61] 100 μM LsRab1 was incubated with 25-fold molar excess of GTP for 1 h at room temperature in 20 mM HEPES (pH 7.5, 150 mM NaCl, 1 mM $MgCl_2$). Free nucleotide was removed with a Buffer exchange A-column (Namo Temper). GTP-loaded LsRab1 proteins were then mixed with RSV NP or TrxA, and the mixture was immediately added to the assay reagents. The final reaction system contained 20 μM LsRab-GTP and 20 μM NP or TrxA. The reaction solution was dispensed into 96-well half-area microplates (Corning, USA), and absorbance at 360 nm was monitored after 20 min-incubation under a microplate spectrometer (Tecan, Switzerland). The concentrations of Pi in the reaction solution were calculated according to the standard curve.

Influence of RSV infection on *L. striatellus* reproduction

To determine the effect of RSV infection on *L. striatellus* reproduction, RSV-free and RSV-infected 5th-instar nymphs were reared separately. After emergence, one female and two males were placed in a glass bottle with five rice seedlings. Eight replicates were performed for each group. Egg numbers on each seedling were counted daily after fertilization. After five days, females were transferred to new glass bottles. The original rice seedlings were maintained, and emerging nymphs were counted daily.

Cell transfection

To observe NP expression effects on LsRab1 localization, the *Drosophila* S2 cell line was used to express NP. Plasmids were transiently transfected into S2 cells using Effectene Transfection Reagent (QIAGEN, Germany) according to the manufacturer's instructions. On transfection day, 1 μg DNA in TE buffer was diluted with Buffer EC to 100 μL. 3.2 μL Enhancer was added and mixed by brief vortexing. After 5–10 min incubation at room temperature, the mixture was added dropwise to cells in 6-well plates. The Effectene-DNA complex was removed at 24 h post transfection. Culture continued for 24 h before subculturing. Protein expression was induced with 0.5 mM $CuSO_4$ 24 h post-subculture and observed by immunofluorescence staining after 48 h of induction.

Cells were fixed with 4% paraformaldehyde at room temperature for 30 min, then treated with an osmotic solution (0.2% Triton X-100 in PBS) for 20 min. Cells were then incubated with LsRab1-, NP-, or GM130-specific antibodies for 1 h, followed by incubation with Alexa Fluor 488-conjugated and Alexa Fluor 568-conjugated antibodies for 1 h.

Phylogenetic construction and bioinformatic analyses

Seabra MC[62] reported Rab family members in *humans*, *Drosophila*, and *yeast*. After downloading Rab protein sequences from the three aforementioned species, these sequences will be aligned with the *L. striatellus* proteome through NCBI BLAST to identify homologous LsRab proteins. The phylogenetic tree was constructed based on the deduced amino acid sequence of LsRab1 and other Rab1s using the neighbour-joining method.[63] Evolutionary analyses were conducted in MEGA6.[64] Bootstrap analysis (1,000 replicates) was applied to generate the rectangular phylogram format. Bootstrap support values above 60% are shown at each node.

Interaction sites between RSV NP and LsRab1 were predicted using AlphaFold 2[65] through ColabFold v1.5.5, which integrates AlphaFold2 with MMseqs2 for sequence alignments and template generation. The full AlphaFold2 pipeline was executed with default parameters, producing five protein-protein interaction models. The rank_001 model, generally considered the most reliable, was selected for this study. The model's accuracy was estimated using two confidence metrics: the predicted Local Distance Difference Test (pLDDT) and the predicted Template Modeling score (pTM). For the LsRab1-RSV NP interaction, the reliability scores were deemed acceptable (pLDDT = 71.4, pTM = 0.571). Visual analysis and interpretation of the AlphaFold 2 predictions were conducted using ChimeraX software.

QUANTIFICATION AND STATISTICAL ANALYSIS

All graphing and statistical analyses were performed using Prism 9.0 software (GraphPad). Data are expressed as the mean ± standard deviation (SD). The differences between the groups were examined by unpaired Student's t-test. *, $p < 0.05$; **, $p < 0.01$; ***, $p < 0.001$; ****, $p < 0.0001$.

Cell Reports, Volume *43*

Supplemental information

Insect-transmitted plant virus balances its vertical transmission through regulating Rab1-mediated receptor localization

Qing Liu, Xiangyi Meng, Zhiyu Song, Ying Shao, Yao Zhao, Rongxiang Fang, Yan Huo, and Lili Zhang

Figure S1

A

```
1   ATGAATCCTGAATATGACTACCTGTTCAAGTTGCTTTTGATTGGAGACTCGGGCGTTGGTAAATCGTGCTTGCTGCTTCGTTTTGCCGAT
1    M  N  P  E  Y  D  Y  L  F  K  L  L  L  I  G  D  S  G  V  G  K  S  C  L  L  L  R  F  A  D
91  GACACATACACGGAAAGTTACATCAGTACTATTGGTGTAGATTTTAAAATTAGAACAATAGATCTCGATGGAAAAACCATAAAGCTCCAG
31   D  T  Y  T  E  S  Y  I  S  T  I  G  V  D  F  K  I  R  T  I  D  L  D  G  K  T  I  K  L  Q
181 ATTTGGGACACAGCCGGCCAGGAACGTTTCCGAACCATCACATCGAGTTACTACAGGGGCGCGCACGGCATCATTGTGGTTTACGACTGC
61   I  W  D  T  A  G  Q  E  R  F  R  T  I  T  S  S  Y  Y  R  G  A  H  G  I  I  V  V  Y  D  C
271 ACCGACCAGGAGTCTTTCAACAATCTGAAACAGTGGCTGGAAGAAATCGACCGCTATGCGTGTGATAATGTCAACAAACTGCTAGTTGGA
91   T  D  Q  E  S  F  N  N  L  K  Q  W  L  E  E  I  D  R  Y  A  C  D  N  V  N  K  L  L  V  G
361 AACAAAAGTGATCAGACCAATAAGAAAGTTGTCGACTACACCCAGGCTAAGGAGTACGCGGACCAGCTGGGCATTCCGTTTCTGGAGACG
121  N  K  S  D  Q  T  N  K  K  V  V  D  Y  T  Q  A  K  E  Y  A  D  Q  L  G  I  P  F  L  E  T
451 TCGGCGAAGAACGCGACCAACGTGGAGCAGGCGTTCATGACAATGGCGGCCGAAATCAAGAACCGCGTCGGGCCGCCGTCGTCCGCAGCC
151  S  A  K  N  A  T  N  V  E  Q  A  F  M  T  M  A  A  E  I  K  N  R  V  G  P  P  S  S  A  A
541 GACACCGCCAACAAGGTGCGCATCAACCAGGCCAGCTCCAGTCCCATCGAGTCCACCAAGTCCGGCTGCTGTTGA
181  D  T  A  N  K  V  R  I  N  Q  A  S  S  S  P  I  E  S  T  K  S  G  C  C  *
```

B

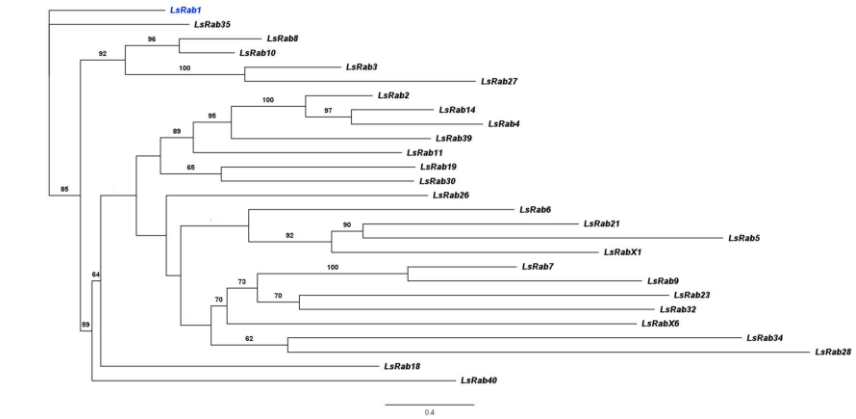

C

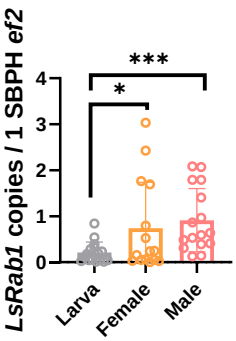

D

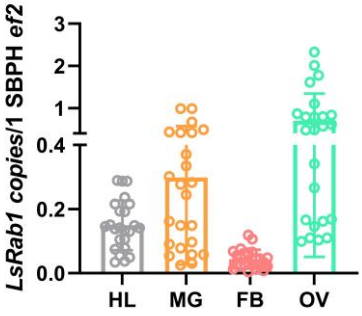

E

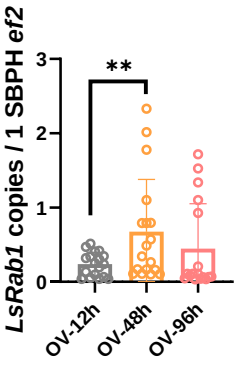

Figure S1. Characteristics of LsRab1 (related to Figure 1). (A) Nucleotide sequence of *LsRab1* and the deduced amino acid sequence of the encoded protein. (B) Phylogenetic analysis of the Rab family proteins in *L. striatellus*. A total of 27 LsRab proteins were aligned, and the phylogenetic tree was constructed using the Neighbor-Joining method. LsRab1 is highlighted in blue. Bootstrap values greater than 60 are indicated at the respective nodes. (C-E) Expression profile of *LsRab1* in different contexts: (C) across various developmental stages of *L. striatellus*, (D) in multiple tissue types, including hemocytes (HL), midgut (MG), fat body (FB), and ovaries (OV), and (E) across distinct ovarian developmental stages. Mean and SD were calculated from three independent experiments using a total of 24 tissue samples. *, $p<0.05$; **, $p<0.01$; ***, $p<0.001$; ****.

Figure S2

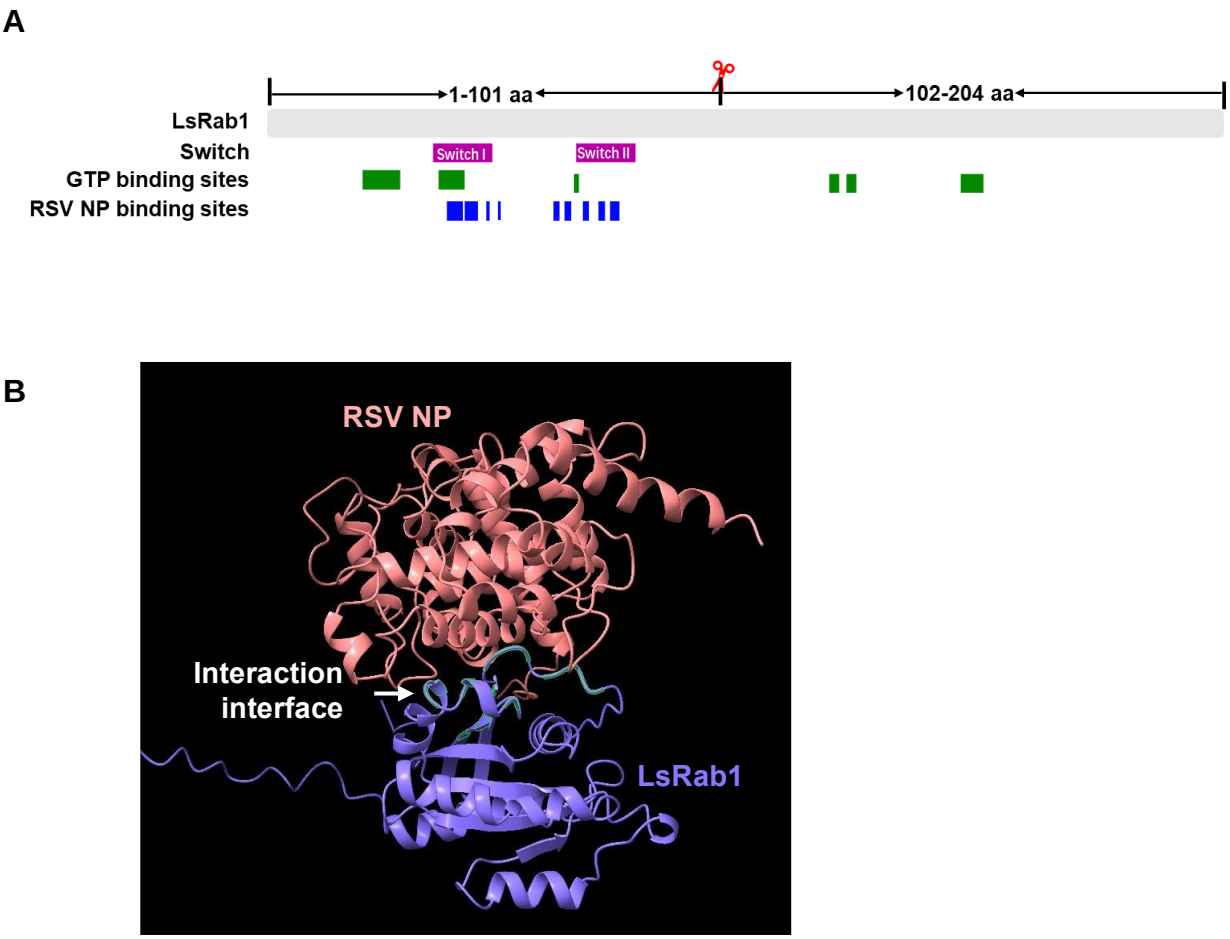

Figure S2. Bioinformatic predictions of the binding sites among LsRab1, GTP, and RSV NP (related to Figure 1). (A) A schematic diagram illustrating the binding sites of Rab1 and GTP (green) in the resolved structure of the Rab1-GTP complex, as well as the predicted interaction sites between LsRab1 and RSV NP (blue) by AlphaFold 2. The Rab1 switch Ⅰ and Ⅱ regions are shown in magenta. These switch regions are crucial for modulating Rab protein activity through interaction with nucleotide molecules. The predicted GTP binding sites include 16D-23C, 33Y-38I, 63D, 121N, 122K, 124D,125L, and 150T-153K.The predicted interaction sites between LsRab1 and RSV NP include LsRab1 (37Y, 38I, 39S, 41I, 42G, 45F, 47I, 60Q, 62W, 67Q, 70F, 72T, and 73I) and RSV NP (47D, 48A, 50T, 115A, 116N, 172E, 210R, 221Y, 224G, 225L, 227V, 228I, 229T, 230C, 231K, 232S, and 233K). (B) Three-dimensional structure of the RSV NP (Pink) and LsRab1 (Purple) complex predicted by AlphaFold 2. The interaction interface in LsRab1 is highlighted in green. .

Figure S3

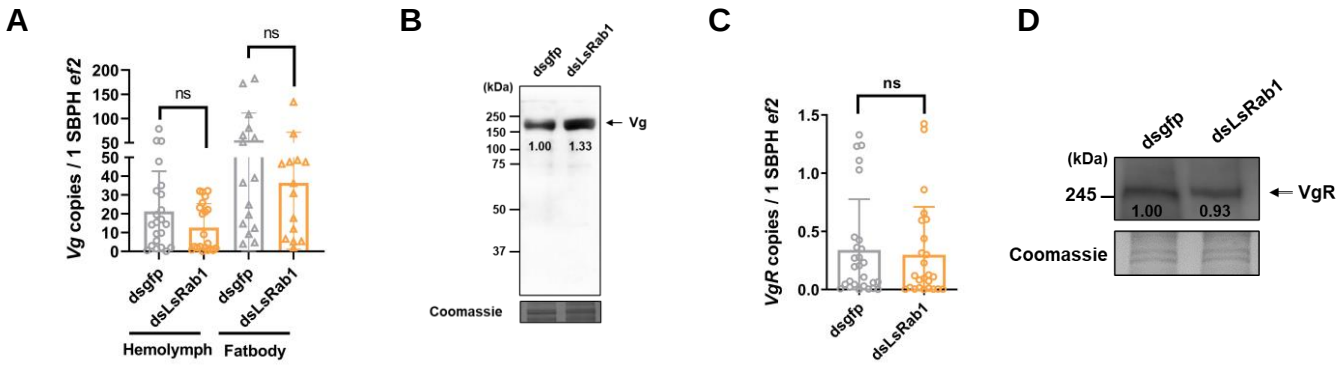

Figure S3. Influence of LsRab1 deficiency on the expression of Vg and VgR (related to Figure 3). (A-B) The impact of LsRab1 deficiency on *Vg* mRNA and protein levels. (C-D) The impact of LsRab1 deficiency on *VgR* mRNA and protein levels. Mean and SD were calculated from three independent experiments. ns, not significant.

Figure S4

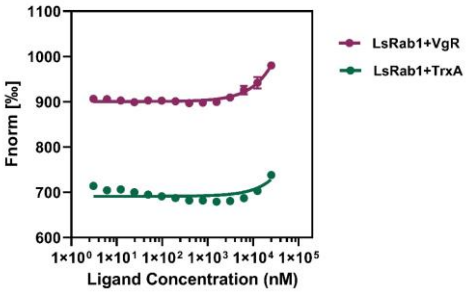

Figure S4. MST assays to determine the interaction between VgR (VgR-CP, amino acids 1797-1927) and LsRab1 (related to Figure 3). TrxA protein is the negative control. Bars represent SD.

Figure S5

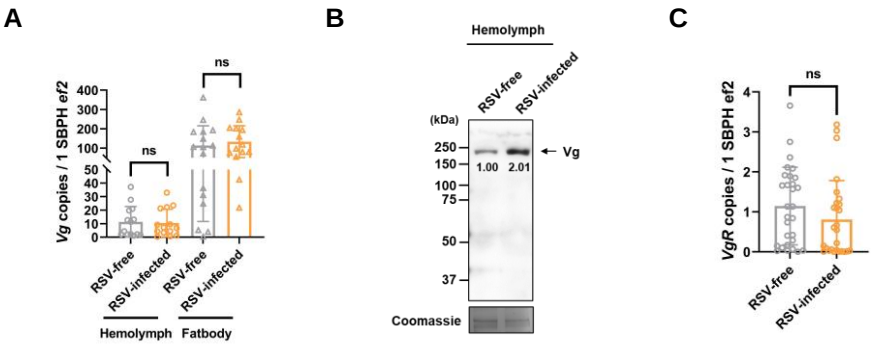

Figure S5. Influence of RSV infection on the expression of Vg and VgR (related to Figure 4). (A) *Vg* mRNA levels in hemocytes or fat body after RSV infection. (B) Vg protein levels in hemolymph after RSV infection. (C) *VgR* mRNA levels in ovaries after RSV infection. Mean and SD were calculated from three independent experiments. ns, not significant.

Figure S6

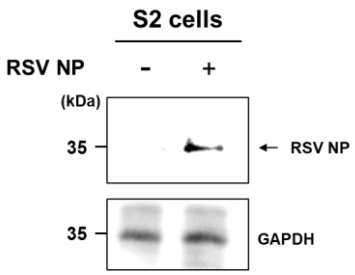

Figure S6. Western blotting analysis of S2 cells following the expression of RSV NP or not (related to Figure 5). S2 cells were transfected with control vector or recombinant pMT-V5-His-NP. Whole S2 cells lysates were detected by western blotting using anti-RSV NP antibody. The immunoblot shown is representative of results obtained in three independent experiments.

Table S1. Co-immunoprecipitation (Co-IP) identification of *L. striatellus* ovarian proteins interacting with RSV RNP in RSV-infected ovaries (related to Figure 1). Proteins present in the negative control group (shown in Table S2) have been eliminated.

Group ID	Protein description	Group ID	Protein description
1	Rab-1A	21	Enolase
2	Ribosomal protein L31	22	Adhesion-regulating molecule 1 precursor
3	Ribosomal protein L23a	23	26S proteasome non-ATPase regulatory subunit 2
4	S14e ribosomal protein	24	Mitochondrial cytochrome c1
5	60S ribosomal protein L10a	25	Cytoskeleton-associated protein 5
6	Ribosomal protein S19e	26	Myotubularin-related protein 10-B
7	60S ribosomal protein L24	27	Beta-tubulin
8	60S ribosomal protein L4	28	Translationally-controlled tumor protein homolog
9	Parcxpwnx05	29	Thioredoxin domain-containing protein 5
10	Histone H2B type 1-M	30	Exuperantia
11	Histone H2A.V	31	Glyceraldehyde-3-phosphate dehydrogenase
12	Histone H2B	32	Transient receptor potential cation channel subfamily A member 1
13	Histone chaperone asf1	33	Pyruvate dehydrogenase phosphatase regulatory subunit, mitochondrial isoform 2
14	Protein TcasGA2	34	Condensin complex subunit 3
15	Cysteine desulfurylase	35	Protein LSM14 homolog B-A
16	Heterogeneous nuclear ribonucleoprotein L	36	Transcription elongation factor SPT6
17	Tetraspanin-31	37	DNA helicase Ino80
18	Uncharacterized protein LOC100888631	38	Regulator of nonsense transcripts 2
19	Dimethyladenosine transferase	39	Vitellogenin
20	Gem-associated protein 5		

Table S2. Proteins from RSV-free *L. striatellus* ovaries that non-specifically bind to RSV RNP antibodies (related to Figure 1).

Group ID	Protein description	Group ID	Protein description
1	Glycerophosphocholine phosphodiesterase GPCPD1	21	Myosin regulatory light chain 2
2	40S ribosomal protein	22	40S ribosomal protein S3a
3	Malate dehydrogenase	23	RNA-binding protein 15B
4	Ribosomal protein S3e	24	V-type proton ATPase subunit H isoform 1
5	Enolase	25	Enoyl-CoA hydratase, mitochondrial
6	ATP synthase subunit beta, mitochondrial	26	Protein disulfide isomerase
7	26S proteasome non-ATPase regulatory subunit	27	F-box/LRR-repeat protein 4
8	Tropomyosin-1	28	Elongation factor 1-alpha
9	Heat shock 70 kDa protein cognate	29	Type I cytokeratin
10	WD repeat domain 35	30	DNA-3-methyladenine glycosylase
11	Trifunctional purine biosynthetic protein adenosine-3	31	Aspartate aminotransferase
12	Ankyrin repeat and zinc finger domain-containing protein 1	32	AGAP004175-PA
13	Glucosamine--fructose-6-phosphate aminotransferase	33	Cytochrome b-c1 complex subunit 2
14	60S ribosomal protein L12	34	Beta-N-acetylglucosaminidase
15	Cytochrome P450	35	Transketolase-like protein 2
16	Hsp90 co-chaperone Cdc37	36	Muscle M-line assembly protein unc-89
17	PHD finger and CXXC domain-containing protein	37	ATP-dependent helicase brm
18	Zinc transporter 9	38	TcasGA2_TC004526
19	26S protease regulatory subunit S10b	39	AP-1 complex subunit gamma-1
20	Fatty acyl-CoA reductase	40	Elongation factor 1-alpha

Table S3. Rab family in different species (related to Figure 1).

L. striatellus	*H. sapiens*	*D. melanogaster*	*S. cerevisiae*
LsRab1	Rab1a,b	DmRab1	Ypt1
LsRab2	Rab2a	DmRab2	
LsRab3	Rab3a,b,d	DmRab3	
LsRab4	Rab4a,b	DmRab4	
LsRab5	Rab5a,b,c	DmRab5	Ypt52,53
LsRab6	Rab6a,b,c	DmRab6	Ypt6
LsRab7	Rab7	DmRab7	Ypt7
LsRab8	Rab8a,b	DmRab8	
LsRab9	Rab9a,b	DmRab9	
LsRab10	Rab10	DmRab10	
LsRab11	Rab11a,b	DmRab11	Ypt31,32
	Rab13		
LsRab14	Rab14	DmRab14	
	Rab17		
LsRab18	Rab18	DmRab18	
LsRab19		DmRab19	
	Rab20		Ypt11
LsRab21	Rab21	DmRab21	
	Rab22a,b		
LsRab23	Rab23	DmRab23	
	Rab24		Ypt10
	Rab25		
LsRab26	Rab26	DmRab26	
LsRab27	Rab27a,b	DmRab27	
LsRab28	Rab28		
	Rab29		
LsRab30	Rab30	DmRab30	
LsRab32	Rab32	DmRab32	
	Rab33a,b		
LsRab34	Rab34		
LsRab35	Rab35	DmRab35	
	Rab36		
LsRab39	Rab39	DmRab39	
LsRab40	Rab40a,b,c	DmRab40	
LsRabX1		DmRabX1	
		DmRabX2	
		DmRabX3	
		DmRabX4	sec4
		DmRabX5	
LsRabX6		DmRabX6	

Rab family proteins identified in *L. striatellus,* along with their counterparts in *Homo sapiens, Drosophila melanogaster,* and *Saccharomyces cerevisiae.*

Table S4. Rab1 GEF (guanine nucleotide exchange factors) associated proteins in *L. striatellus* (related to Figure 2).

Protein (Human)	Protein (Yeast)	Gene	*Drosophila melanogaster* CG number	Length (AA)	*Laodelphax striatellus* LSTR number	Length (AA)	Identities/positives/Gaps
TRAPPC6	Trs33	*Trs33*	Dmel_CG6196	152	LSTR_LSTR002995	163	57%, 80%, 3%
TRAPPC2	Trs20	*Trs20*	Dmel_CG5161	139	LSTR_LSTR008180	140	67%, 83%, 0%
TRAPPC5	Trs31	*Trs31*	Dmel_CG10153	194	LSTR_LSTR009402	191	69%, 85%, 0%
TRAPPC4	Trs23	*Trs23*	Dmel_CG9298	219	LSTR_LSTR001144	217	73%, 87%, 0%
TRAPPC3	Bet3	*Bet3*	Dmel_CG3911	178	LSTR_LSTR003084	178	68%, 84%, 0%
TRAPPC1	Bet5	*Bet5*	Dmel_CG1359	145	LSTR_LSTR000460	144	70%, 83%, 0%

Table S5. Primers used in this study.

Primer name (F, forward primers; R, reverse primers)	Primer sequence (5'-3')	Primer description
Primers for RT-qPCR:		
LsRab1-qF	AGACTCGGGCGTTGGTAAA	For gene expression analysis of *LsRab1*
LsRab1-qR	AAAGACTCCTGGTCGGTGC	
EF2-qF	GTCTCCACGGATGGGCTTT	For gene expression analysis of *EF2*
EF2-qR	ATCTTGAATTTCTCGGCATACATTT	
RSV NP-qF	GATGAAGTACACAACTGGTC	For *RSV NP* amplification analysis
RSV NP-qR	AGTGCTGATCGTATTGACAGA	
VgR-qF	AAACGCCTAATGGACCTAAATGC	For gene expression analysis of *VgR*
VgR-qR	CGAGTAGACAATACCCAGATACGAGTG	
Vg-qF	TGGGTATGCACATGAAAGC	For gene expression analysis of *Vg*
Vg-qR	CCTAGACTTGATGGCGTTCT	
TRAPPC5-qF	TCGCCCGAAAAGTATCCTGG	For gene expression analysis of *TRAPPC5*
TRAPPC5-qR	AACGCCAACTTCTTGTCCCA	
Primers for expression plasmid construction:		
LsRab1-F	ATGAATCCTGAATATGACTACC	For gene amplification of *LsRab1*
LsRab1-R	ACAGCAGCCGGACTTGGT	
pET30a-LsRab1-F	TTTAAGAAGGAGATATACATATGATGAATCCTGAATATGACTACC	For expression plasmid construction of LsRab1-His
pET30a-LsRab1-R	TGGTGGTGGTGGTGGTGCTCGAGACAGCAGCCGGACTTGGT	
NP-F	ATGGGTACCAACAAGCCAGC	For gene amplification of *RSV NP*
NP-R	CTAGTCATCTGCACCTTCTG	
pET30a-NP-F	TTTAAGAAGGAGATATACATATGGGTACCAACAAGCCAGC	For expression plasmid construction of RSV NP-His
pET30a-NP-R	TGGTGGTGGTGGTGGTGCTCGAGCTAGTCATCTGCACCTTCTG	
pGEX-3X-NP-F	GGATCCCCATGGGTACCAACAAGCCAGC	For expression plasmid construction of RSV NP-GST
pGEX-3X-NP-R	CCCGGGCTAGTCATCTGCACCTTCTG	
Primers for RNAi:		
dsgfp-F	ATGGTAGATCTGACTAGTAA	For synthesis of *dsgfp* templates
dsgfp-R	CTAGTCATCTGCACCTTCTG	
dsgfp-T7F	TAATACGACTCACTATAGGATGGTAGATCTGACTAGTAA	For synthesis of *dsgfp* templates
dsgfp-T7R	TAATACGACTCACTATAGGCTAGTCATCTGCACCTTCTG	
dsLsRab1-F	TGCTGCTTCGTTTTGCCGAT	For synthesis of *dsLsRab1* templates
dsLsRab1-R	GACGTCTCCAGAAACGGAATG	
dsLsRab1-T7F	TAATACGACTCACTATAGGTGCTGCTTCGTTTTGCCGAT	For synthesis of *dsLsRab1*
dsLsRab1-T7R	TAATACGACTCACTATAGGGACGTCTCCAGAAACGGAATG	
dsTRAPPC5-F	TAGCTTGAGCTGTTTTGCCC	For synthesis of *dsLsTRAPPC5* templates
dsTRAPPC5-R	CCTTTGTGCCAATGAGCTGTT	
dsTRAPPC5-T7F	TAATACGACTCACTATAGGTAGCTTGAGCTGTTTTGCCC	For synthesis of *dsLsTRAPPC5*
dsTRAPPC5-T7R	TAATACGACTCACTATAGGCCTTTGTGCCAATGAGCTGTT	